Materials Today Bio 13 (2022) 100192

Contents lists available at ScienceDirect

Materials Today Bio

journal homepage: www.journals.elsevier.com/materials-today-bio

ROS-responsive nanoparticle-mediated delivery of CYP2J2 gene for therapeutic angiogenesis in severe hindlimb ischemia

Liang Gui [a,b,d,1], Youlu Chen [c,1], Yongpeng Diao [a], Zuoguan Chen [a], Jianwei Duan [c], Xiaoyu Liang [c], Huiyang Li [c], Kaijing Liu [c], Yuqing Miao [a], Qing Gao [a], Zhichao Li [a], Jing Yang [c,**], Yongjun Li [a,*]

[a] Department of Vascular Surgery, Beijing Hospital, National Center of Gerontology; Institute of Geriatric Medicine, Chinese Academy of Medical Science and Peking Union Medical College, Beijing, 100730, PR China
[b] Graduate School of Peking Union Medical College, Beijing, 100730, PR China
[c] Tianjin Key Laboratory of Biomaterial Research, Institute of Biomedical Engineering, Chinese Academy of Medical Sciences and Peking Union Medical College, Tianjin, 300192, PR China
[d] Department of Vascular Surgery, The First Affiliated Hospital of Nanjing Medical University, Nanjing, Jiangsu, 210029, PR China

ARTICLE INFO

Keywords:
Therapeutic angiogenesis
Gene therapy
Nanocarriers
CYP2J2
Hindlimb ischemia

ABSTRACT

With critical limb ischemia (CLI) being a multi-factorial disease, it is becoming evident that gene therapy with a multiple bio-functional growth factor could achieve better therapeutic outcomes. Cytochrome P450 epoxygenase-2J2 (CYP2J2) and its catalytic products epoxyeicosatrienoic acids (EETs) exhibit pleiotropic biological activities, including pro-angiogenic, anti-inflammatory and cardiovascular protective effects, which are considerably beneficial for reversing ischemia and restoring local blood flow in CLI. Here, we designed a nanoparticle-based pcDNA3.1-CYP2J2 plasmid DNA (pDNA) delivery system (nanoparticle/pDNA complex) composed of a novel three-arm star block copolymer (3S-PLGA-po-PEG), which was achieved by conjugating three-armed PLGA to PEG via the peroxalate ester bond. Considering the multiple bio-functions of CYP2J2-EETs and the sensitivity of the peroxalate ester bond to H_2O_2, this nanoparticle-based gene delivery system is expected to exhibit excellent pro-angiogenic effects while improving the high oxidative stress and inflammatory micro-environment in ischemic hindlimb. Our study reports the first application of CYP2J2 in the field of therapeutic angiogenesis for CLI treatment and our findings demonstrated good biocompatibility, stability and *sustained release* properties of the CYP2J2 nano-delivery system. *In addition, this nanoparticle-based gene delivery system showed high transfection efficiency and efficient VEGF expression in vitro and in vivo. Intramuscular injection of nanoparticle/pDNA complexes into mice with hindlimb ischemia resulted in significant rapid blood flow recovery and improved muscle repair compared to mice treated with naked pDNA.* In summary, 3S-PLGA-po-PEG/CYP2J2-pDNA complexes have tremendous potential and provide a practical strategy for the treatment of limb ischemia. Moreover, 3S-PLGA-po-PEG nanoparticles might be useful as a potential non-viral carrier for other gene delivery applications.

1. Introduction

Peripheral artery disease (PAD) is a common disease worldwide and often related to high morbidity and mortality, especially critical limb ischemia (CLI) [1]. Traditional surgical procedures or endovascular revascularization is feasible and efficient therapeutic option for general patients; however, approximately 30% of patients do not have access to surgical or interventional operation because of the complicated anatomy of the vascular occlusion or severe comorbidities, making non-surgical treatment particularly important [2,3].

Both basic and clinical studies have demonstrated the biological effectiveness of gene therapy with pro-angiogenic factors for CLI and the

Abbreviations: CLI, critical limb ischemia; PAD, peripheral artery disease; CYP2J2, cytochrome P450 epoxygenase 2J2; EETs, epoxyeicosatrienoic acids; ROS, reactive oxygen species.

* Corresponding author. No. 1 Dahua Road, Dong Dan, Beijing, 100730, PR China.
** Corresponding author. No. 236 Baidi Road, Nankai District, Tianjin, 300192, PR China.
E-mail addresses: yangjing37@hotmail.com (J. Yang), liyongjun4679@qq.com (Y. Li).
[1] These authors contributed equally to this work.

https://doi.org/10.1016/j.mtbio.2021.100192
Received 23 September 2021; Received in revised form 7 December 2021; Accepted 17 December 2021
Available online 20 December 2021

advantages of lower cost and longer half-life compared to the direct application of cytokines or growth factors, such as vascular endothelial growth factor (VEGF), fibroblast growth factor (FGF) and hepatocyte growth factor (HGF) [4–6]. Among multitudinously investigated growth factors, gene therapy with HGF holds greater promise than therapy with other growth factors, which can be explained by the fact it promotes angiogenesis while inhibiting inflammation and cellular senescence [7]. Due to the multiple factors involved in the process of CLI, it is increasingly reasonable and necessary to efficiently deliver a multiple bio-functional gene or more than one gene to target cells.

Gene delivery is carried out by various developed viral or non-viral vectors. To date, mainly due to high transfection efficiency and extended plasma presence half-life, viral vectors have been extensively applied [8]; however, the potential cellular toxicity and immune response that accompany viral insertional mutagenesis may result in a few safety issues [9]. Relying on high biocompatibility and good sustained-release properties, nanoparticle-based gene delivery systems have the ability to address these shortcomings and pave the way for therapeutic options that are safer than viral vectors [10].

As a non-viral vector, poly (lactic-*co*-glycolic acid) (PLGA) nanospheres have been approved by the US Food and Drug Administration (FDA) and are widely used in the biomedical field by virtue of their excellent biodegradability and reliable safety [11]. Linking polyethylene glycol (PEG) to PLGA not only dramatically improves the hydrophilicity of PLGA, but also greatly extends the cycle time of drugs *in vivo* [12]. Excessive reactive oxygen species (ROS) play a key role in the pathogenesis and progression of CLI by causing endothelial dysfunction and oxidative damage to myofibers, indicating a therapeutic option concentrated on ROS regulation [13–15]. Peroxalate derivatives are usually obtained by reacting oxalyl chloride with two chemical groups bearing phenol group and can only react with hydrogen peroxide (H_2O_2), a major ROS member [16]. Thus, we innovatively synthesized a novel three-arm star block copolymer (3S-PLGA-po-PEG) with peroxalate ester (PO) as an H_2O_2-responsive linkage through the esterification reaction of oxalyl chloride and hydroxyl groups. In addition, our previous *in vitro* findings revealed the good biocompatibility, sustained-release and H_2O_2-scavenging properties of 3S-PLGA-po-PEG as a drug-delivery vehicle [17, 18].

As a known arachidonic acid (AA) epoxygenase, Cytochrome P450 epoxygenase (CYP) mediates the formation of four bioactive regioisomers of epoxyeicosatrienoic acids (EETs): 5, 6-EET, 8, 9-EET, 11, 12-EET, and 14, 15-EET. CYP2J2 is the only member of human CYP2J subfamily and is mainly expressed in endothelial cells and myocardial cells [19,20]. Quite a few studies have shown that CYP2J2 and its catalytic product EETs exert pro-angiogenic and anti-inflammatory properties while inhibiting endothelial cell apoptosis *in vitro*, which are considerably beneficial activities to reverse ischemia and restore local blood flow in CLI [21–23]; however, few *in vivo* investigations of the actual therapeutic effect of CYP2J2 and EETs in CLI have been performed.

In this study, we designed a CYP2J2 DNA delivery system using 3S-PLGA-po-PEG nanoparticles as a gene vector, with the goal of achieving high transfection efficiency and appropriate H_2O_2 scavenging. The coding DNA fragment of CYP2J2 was subcloned into a pcDNA3.1 plasmid, and the generated engineered plasmid DNA (pDNA) was loaded into 3S-PLGA-po-PEG to explore the efficiency of CYP2J2 and EETs expression. A mouse limb ischemic model was established to evaluate the pro-angiogenic ability of this gene delivery system. In addition, we explored the potential molecular mechanism of CYP2J2-EETs pro-angiogenic activity.

2. Experimental section

2.1. Preparation of 3s-PLGA-po-PEG nanoparticles

3S-PLGA: First, 1.304 g stannous octoate ($SnOct_2$; Sigma-Aldrich, St Louis, MO, USA) was dissolved in dry dichloromethane (CH_2Cl_2; Jiangtian Chemical Technology Co Ltd., Tianjin, China) at a concentration of 30.56 mmol/L. A mixture of $_{D,\ L}$-Lactide (4.32 g, 30 mmol; Glaco Ltd., Beijing, China), glycolide (GA, 1.16 g, 10 mmol; Glaco Ltd., Beijing, China), propanetriol (18.4 mg, 0.2 mmol; Guangfu Fine Chemical Research Institute, Tianjin, China) and the above SnOct2 solution (0.523 mL, 0.004 mmol) was added into a 50 mL polymerization tube. After that, the polymerization tube was evacuated and filled with argon (three times). Then, approximately 30 min of evacuation was applied to thoroughly remove the air and CH_2Cl_2 in the tube. Following this, the polymerization tube was sealed and placed into a vacuum oven at 160 °C for 8 h, and then allowed to cool to room temperature (RT). The reaction product was dissolved in CH_2Cl_2 and purified by precipitation in iced methanol three to four times. Finally, 3S-PLGA was dried in vacuum at RT until a constant weight was verified (4.80 g, 87.5%).

3S-PLGA-po-PEG: Oxalyl chloride (0.417 g, 3.28 mmol; Guangfu Fine Chemical Research Institute, Tianjin, China) was dissolved in 10 mL of anhydrous CH_2Cl_2 in a 100 mL round-bottom flask, and then, an anhydrous CH_2Cl_2 solution of PEG (1.32 g, 0.328 mmol; Guangfu Fine Chemical Research Institute, Tianjin, China) was added dropwise into the flask, and stirring was maintained for 3 h under a nitrogen atmosphere in an ice-bath. After the reaction, CH_2Cl_2 and excess oxalyl chloride were removed by evaporation under reduced pressure. The evaporated solid was re-dissolved with dichloromethane and re-evaporated 3–4 times to completely remove residual oxalyl chloride. Afterward, the residue was dissolved in 20 mL of anhydrous dichloromethane in a flask, and an anhydrous CH_2Cl_2 solution of triethylamine (0.017 g, 0.164 mmol) and 3S-PLGA (1 g, 0.036 mmol) was added dropwise into the flask under stirring. After reaction for 48 h at room temperature under a nitrogen atmosphere, the mixture was filtered to remove insoluble matter, and washed 3 times with 1 M HCl and saturated NaCl respectively. Then, the organic solution was dried over anhydrous $MgSO_4$. After removal of the $MgSO_4$ by filtration, the filtrate was steamed and concentrated, and then dropped into cold anhydrous ether to precipitate for solid substance. The solid substance was washed 3–4 times with cool methanol to remove excess PEG. The product was dried to constant weight in a vacuum drying oven at 40 °C.

2.2. Construction of plasmid

The CYP2J2 cDNA (1.876 kilobase pairs; GenBank accession number: U37143) and enhanced green fluorescent protein (eGFP) cDNA were both inserted into pcDNA3.1 plasmid according to previous studies [21, 24]. The plasmids containing CYP2J2 and eGFP were purified with a QIAGEN Plasmid Maxi Kit (QIAGEN, Inc., Chatsworth, CA) following the instructions of the manufacturer.

2.3. Construction of nanoparticle/pDNA complexes

Under stirring at 20,000 rpm in an ice bath, 1 mL of ultrapure water containing 1 mg protamine was slowly added dropwise to a 2 mL dichloromethane solution containing 80 mg 3s-PLGA-po-PEG nanoparticles, and then plasmid solution containing 1.5 mg pcDNA3.1-CYP2J2 plasmid was added into the above suspension. The mixture was added to 1% Polyvinyl alcohol (PVA) under high-speed stirring, and then stirred and evaporated at room temperature (RT) for 3 h. The dichloromethane was removed by evaporation to obtain nanoparticle/plasmid complexes.

2.4. Physiochemical characterization

The mean particle size, size distribution (PDI), and zeta potential of the nanoparticle/pDNA complexes were determined via dynamic light scattering (DLS) on a Zeta-sizer Nano ZS (Malvern Instruments, Malvern, UK). In addition, the transmission electron microscope (TEM; Tianjin Research Center of Basic Medical Science) was employed to analyze the morphology and size of the nanoparticle/pDNA complexes. All

experiments were repeated three times with three parallels for each sample.

2.5. Agarose gel retardation assay for structural integrity

The pDNA extracted from the nanoparticles was examined to assess the purity and structural integrity before and after encapsulation. The pDNA was extracted from the nanoparticles using 1 N NaOH. In brief, the products mixed with 6 × DNA-loading buffer (Fermentas, Ontario, Canada) were loaded into 1% Tris-acetate-EDTA (TAE) buffer containing 0.5 μg/mL ethidium bromide (Sigma-Aldrich, Stockholm, Sweden). The samples were electrophoresed at 70 V for 30 min and the result was analyzed using a gel imaging system (Bio-Rad, Hercules, CA, USA).

2.6. Release kinetics of pDNA in vitro

In brief, 20 mg pDNA-loaded nanoparticles were suspended in 2 mL of PBS or H_2O_2 solution (40 μmol/L) under continuous stirring. At designated time points, the supernatant was removed, and an equal volume of fresh buffer was replenished. The DNA concentration in the supernatant was measured on an ultraviolet spectrophotometer (Hitachi, Tokyo, Japan). The experiments and measurements were carried out in triplicate.

2.7. Cell lines and cell culture

Human aortic endothelial cells (HAECs) were purchased from National Infrastruction of Cell Line Resource (Beijing, China). HAECs were grown in medium ECM (ScienCell, CA, USA) containing endothelial cell growth supplements (ECGSs), 100 units/ml penicillin and 100 mg/mL streptomycin. The cultures were maintained in saturated humidity with 5% CO_2 at 37 °C and cells were used at passages 5–7 to perform the experiments. Short tandem repeat (STR) profiling was performed to ensure cell identity.

2.8. Intracellular ROS scavenging ability

To observe the intracellular ROS scavenging ability of nanoparticle/pDNA complexes, the LPS-induced intracellular ROS generation by HAECs was detected with the ROS sensitive fluorescent dye dichlorofluorescein diacetate (DCFH-DA; Solarbio, Beijing, China). Briefly, cells in 24-well plates were pretreated with LPS (5 μg/mL) for 4 h and then treated with PBS, blank nanoparticles or nanoparticle/pDNA complexes. DCFH-DA was used to determine the intracellular ROS level. Finally, observations were performed using a laser scanning confocal microscope (LSCM; ZEISS-LSM 700, Jena, Germany).

2.9. Cytotoxicity assay

The cytotoxicity of nanoparticle/plasmid complexes toward HAECs was examined using the Cell Counting Kit-8 (CCK-8; Dojindo Laboratories, Shanghai, China) reagent. Cells were seeded (5×10^3 cells/well) into 96-well plates and incubated for 24 h at 37 °C. Then, the cells were treated with blank nanoparticles, naked pDNA or nanoparticle/pDNA complexes. Lipofectamine 2000 was used as the positive control, and untreated cells were considered as the negative control. After 24 h, the medium was exchanged with whole medium, and the cells were incubated for another 48 h. Thereafter, 10 μL of CCK-8 reagent was added to each well and incubated with the cells at 37 °C for 4 h. Optical density (OD) was measured at 450 nm using a Varioskan Flash microplate reader (Multiskan FC, Thermo Fisher Scientific Inc., Waltham, MA, USA). All experiments were performed in triplicate.

2.10. Cellular uptake and endo/lysosomal escape

Cellular uptake and lysosomal escape of the nanosphere/plasmid complex were determined using LSCM. HAECs were seeded in a confocal dish at a density of 2×10^5 cells per well and cultured for 24 h. A total of 1 mL coumarin-6 (green fluorescent dye) labeled blank-nanoparticles were prepared and added to cell cultures for 2 h or 4 h incubation. Then, the cells were incubated with 1 mL LysoTracker Red (Beyotime, Shanghai, China) for 120 min at 37 °C. Subsequently, samples were washed with PBS three times and 500 μl 4% paraformaldehyde (PFA) was added to fix HAECs at RT for 20 min. Finally, the cells were incubated with DAPI (1 μg/mL) for nuclear staining at RT for 5 min and observed via LSCM.

2.11. Gene transfection efficiency in vitro

HAECs were seeded (2×10^5 cells) into a confocal dish and cultured for 24 h. When cells reached 60–70% confluence, 1 mL nanoparticle/plasmid complexes (166.75 μg/mL) was added into each dish for 48 h of transfection. eGFP was employed as a reporter gene to assess the gene transfection efficiency of nanosphere/plasmid complexes under LSCM. Additionally, the transfection efficiency was also tested by examining the expression of CYP2J2 protein using ELISA assay (Signalway Antibody; College Park, MD, USA). Lipofectamine 2000 (Invitrogen, CA, USA) with pDNA served as a positive control (Lipo) and untreated HAECs were used as the negative control.

2.12. Cell migration assay

A scratch test was performed to evaluate the migration ability of HAECs treated with nanoparticle/pDNA complexes (166.75 μg/mL). HAECs were seeded (1×10^5 cells/well) into 6-well plates and cultured for 24 h. The cell monolayers were carefully and evenly scratched using a sterile pipette tip, and each well was washed three times with PBS to remove cell fragments. Then, the cells were treated with PBS, blank nanoparticles, naked pDNA or nanoparticle/pDNA complexes and incubated at 37 °C. Optical microscope (Olympus, BX61; Tokyo, Japan) images were captured at 0, 24 and 48 h. Quantification of migration efficiency was performed using NIH Image J sofeware (Bethesda, MD, USA) and calculated as follows: % Cell migration $= (S_0 - S_t)/S_0 \times 100$ (S_0: scratch wound area at 0 h; S_t: scratch wound area without cell migration at 24 or 48 h).

2.13. Tube formation assay

A tube formation assay was performed as described in a previous study [25]. Briefly, 150 μl Matrigel (BD Bioscience) was left to solidify onto each well of a pre-cooled 24-well tissue culture plates (Ibidi, Germany) for 30 min at 37 °C. Subsequently, HAECs were digested with 0.25% trypsin, and a single-cell suspension was prepared. A total of 5×10^4 cells in a total volume of 500 μl of cell suspension were added to each well and incubated with nanoparticles/pDNA (166.75 μg/mL) at 37 °C for 6 h. Finally, tube formation was observed under an inverted fluorescence microscope (Nikon, Tokyo, Japan), and 5 microscope fields were randomly selected for analysis in each viewed sample. The total tube length was measured using Image J sofeware.

2.14. Creation of hindlimb ischemia in mouse model

All animal experiments were performed in accordance with Peking Union Medical College Animal Care and Use Committee guidelines. Female ICR mice (6 weeks old, weighing 24–27 g) were purchased from SPF Biotechnology co., LTD. Under peritoneal anesthesia with 4% chloral

hydrate (0.1 mL/10 g), the left femoral artery was ligated using 8–0 polyamide nylon sutures at the distal end of the external iliac artery and proximal end of the iliac artery; subsequently, the femoral artery between the two ligation points was excised. Laser Doppler imaging analysis of the ischemic limb on the first postoperative day was conducted to confirm the success of the operation. Mice were randomly assigned to four groups based on different treatments: control group (Control), blank-nanoparticle group (Blank-NP), naked pDNA group (pDNA) and nanoparticle/pDNA complexe group (NP/pDNA). On postoperative days 1, 3 and 5, a total volume of 75 μl of nanoparticle/pDNA complexes (concentration: 166.75 μg/mL, containing 5.025 μg pcDNA 3.1-CYP2J2 plasmid) was injected at four sites into gastrocnemius and soleus in the NP/pDNA group. The control group, NP group and pDNA group were respectively injected with PBS (75 μl), blank nano-emulsion (75 μl) or liquid plasmid (75 μl, containing 5.025 μg pcDNA 3.1-CYP2J2 plasmid) at the designated time points.

2.15. Laser Doppler blood perfusion measurement

Blood perfusion of the hindlimb was measured with a Laser Doppler Perfusion Imager (LDPI, Moor Instruments, Devon, Sweden) 0, 7, 14, 21 and 28 days after treatment to evaluate the neovascularization in ischemic hindlimbs. Before measurement was started, the mice were placed on a warm plate at 37 °C to avoid variations in blood flow caused by the ambient temperature and light. The limb perfusion ratio was calculated based on the ratio of left (ischemic) to right (non-ischemic) hindlimbs.

2.16. In vivo small animal imaging

The mouse model of hindlimb ischemia was generated as described above. A total of 75 μl coumarin-6-labeled blank nanoparticles (166.75 μg/mL) were injected into the ischemic gastrocnemius muscle one day post-surgery. The fluorescence signals of coumarin-6 (excitation: 466 nm; emission: 504 nm) were monitored using a small animal live body imager (PhotonIMAGER, BiospaceLab, France) at various time points after intramuscular injection.

2.17. Histological analysis

After the LDPI measurements were finished on day 28, all the mice were euthanized via anesthesia with an overdose of chloral hydrate. The gastrocnemius muscles were extracted and immediately fixed in 4% paraformaldehyde for 24 h. Tissue samples were paraffin-embedded and cut into 4-μm sections. Each section was stained with hematoxylin-eosin and Masson's trichrome for morphological analysis and fibrosis evaluation. For CD31 staining, sections were stained with the relevant antibody (1:100, no. ab182981, Abcam, Cambridge, UK). Finally, the sections were observed under an optical microscope. Five random views were selected and evaluated by two blinded experienced investigators.

2.18. Immunofluorescence

Neovessels were evaluated using double immunofluorescence staining of CD31 and alpha smooth muscle actin (α-SMA). Rehydrated sections were washed three times with TBS and incubated in blocking solution for 30 min. Then, the sections were incubated with anti-CD 31 antibody (1:100, no. ab182981, Abcam) and anti-α-SMA antibody (1:100, no. ab7817, Abcam) at 4 °C overnight. Anti-mouse Alexa 546 (Invitrogen, 1:250) and anti-rabbit Alexa 488 (Invitrogen, 1:250) secondary antibodies were then applied. After the slides were washed three times with TBS for 3 × 5 min, nuclei were stained with DAPI, and the sections were observed via LSCM. The number of double-positive labeling of CD-31 and α-SMA vascular structures was analyzed and documented.

2.19. Western blotting analysis

Western blotting was conducted to measure the protein level of CYP2J2/VEGF/HIF-1α/eNOS in the gastrocnemius muscle after treatments. Gastrocnemius tissue was separated and immediately snap-frozen in liquid nitrogen and stored at −80 °C. Muscle tissue was homogenized in RIPA lysis buffer (Beyotime, China) following the instructions of manufacturer and centrifuged at 12,000 rpm for 10 min at 4 °C. Protein concentrations were examined using a BCA Protein Assay Kit (Beyotime, China), and equal amounts of protein were separated via SDS-PAGE and then transferred to PVDF membranes. Membranes were blocked in TBST (Tris-buffered saline containing 0.1% Tween-20) with 5% skim milk at RT for 1 h and incubated with primary antibody (1:500 dilution) at 4 °C overnight. Then, the membranes were washed three times with TBST and incubated for 1 h with corresponding secondary antibody (1:2000 dilution). The intensities of the immunoblotted bands were normalized against GAPDH, and the signal was developed using digital image software (Kodak, USA).

2.20. Real-time PCR analysis

Total RNA was harvested from HAECs using TRIZOL (Invitrogen). First-stranded cDNA was synthesized from 1 μg of total RNA using an RT2 First Strand Kit (Qiagen). Then the cDNA was amplified via PCR with specified primers and EasyTaq PCR Mix (Transgen Biotech, Beijing, China) in a volume of 20 μl following the manufacturer's instructions. The primers were as follows: HIF-α, (F) 5′-CTCGGCGAAGCAAAGAG-3′ and (R) 5′-GCCATCTAGGGCTTTCAG-3′; GAPDH, (F) 5′-TGACCGGGTCACCCACACTGTGCCCATCTA-3′ and (R) 5′-CTAGAA GCATTTGCGGTG GACGATGGAGGG-3′. Gene expression was presented as the fold change relative to the GADPH mRNA expression, and experiments were conducted using a 7500 Real-Time PCR System (Applied Biosystems; Thermo Fisher Scientific, Waltham, MA, USA).

2.21. ELISA assay

EETs are highly unstable within the organisms and are quickly hydrolyzed to the corresponding stable metabolite dihydroxyeicosatrienoic acids (DHETs) by soluble epoxide hydrolases (sEHs). To assess EETs production, an ELISA kit (Detroit R&D, Detroit, MI) was used to determine the concentrations of the stable EETs metabolite-DHETs according to the manufacturer's instructions, as previously described [23,26]. Concentrations of IL-1β and IL-6 in ischemic tissues were also measured by using commercial ELISA kits (Thermo Fisher Scientific, Paisley, UK) according to the technical guide protocol, and the results were calculated based on the standard curve and expressed as pg/mg.

2.22. H_2O_2 detection

The levels of H2O2 in ischemic muscle were detected using the Hydrogen Peroxide Assay Kit (Beyotime Biotechnology, Shanghai, China) according to the manufacturer's protocol. Briefly, the muscle tissue was homogenized and centrifuged at 12,000 rpm for 5 min, and the supernatant was collected for further research. Samples were placed into a 96-microwell plate for UV detection and the OD was measured at 560 nm using a microplate reader. The concentration of H2O2 in each sample was calculated according to the standard curve.

2.23. Statistical analysis

Data are shown as the mean ± SD. Statistical significance was evaluated using One-way analysis of variance (ANOVA), and the Bonferroni post-test was used for comparisons between groups. All statistical analyses were conducted using software SPSS version 20.0 software (SPSS Inc., Chicago, IL, USA). $P < 0$ 0.05 was considered statistically significant.

3. Results

3.1. Preparation and characterization of nanoparticle/pDNA complexes

In this study, we evaluated a potential approach to constructing a therapeutic nanoparticle/pDNA complexes for the treatment of CLI. Firstly, the three-arm star block copolymer-3S-PLGA-po-PEG was synthesized through ring-opening polymerization and esterification of oxalyl chloride. Characterization of 3S-PLGA-po-PEG was displayed in Figure S1, and the results were consistent with those of our previous studies [17,27]. Although nanopolymer-mediated gene delivery has the advantages of good biocompatibility and slow-release ability, it has limitations with regard to noteworthy transfection efficiency and cellular uptake. As a solution, surface modification of nanospheres with protamine was performed to improve the drug-loading and decrease the negative surface charge of nanoparticle/pDNA complexes.

As shown in Fig. 1b and c, the negative charge of pDNA and increased repulsion forces between nanoparticles resulted in a decrease in particle size, from 246 ± 5.9 nm (Blank-NP) to 210 ± 3.5 nm (NP/pDNA), and in zeta potentials from −7.2 ± 0.19 mV (Blank-NP) to −13.9 ± 0.55 mV (NP/pDNA). TEM analysis demonstrated nearly spherical outline and uniform size of nanoparticle/pDNA complexes (Fig. 1d/I). Furthermore, in the presence of H_2O_2 (200 μM), irregular morphology and aggregation of nanoparticle/pDNA complexes were observed instead (Fig. 1d/II), caused by PO bonds breakage and NPs bursting in response to H_2O_2. Next, the stability of nanoparticle/pDNA complexes was evaluated by monitoring changes in their size and distribution at various time points. The mean particle size increased slightly, from 210 nm to 235 nm, while the zeta potentials and PDI did not change substantially. As an estimate of pDNA purity and structural integrity, gel electrophoresis assay was carried out and the results clearly suggested that there was no significant change before and after encapsulation of pDNA (Fig. 1f). In PBS, nanoparticle/pDNA complexes showed a 26.3% release of the encapsulated pDNA within 24 h, followed by sustained release of 80% over 9 days (Fig. 1g). In contrast, in H_2O_2 solution (40 μM) there was an initial release burst in the first 24 h with 39.3% release of pDNA and sustained release of 92.3% over 9 days (Fig. 1g). According to previous studies [28], a 40 μM H_2O_2 concentration was chosen to mimic the *in vivo* ischemic micro-environment. Additionally, the release kinetics of pDNA from nanoparticle/pDNA complexes at higher concentration of H_2O_2 (200 μM) was also determined. In 200 μM H_2O_2, there was an initial burst release in the first 6 h with 54.8% release of pDNA and sustained release of 93.1% over 2 days (Figure S1-d). All these findings showed good H_2O_2-sensitivity of NP/pDNA. Moreover, intracellular ROS scavenging ability of nanoparticle/pDNA complexes was tested utilizing ROS probe DCFH-DA. As shown in Fig. 1h, intracellular ROS generation was significantly increased after LPS stimulation and the addition of blank-nanoparticles and nanoparticle/pDNA complexes efficiently reduced the fluorescence signal, directly indicating the good intracellular ROS scavenging ability of 3S-PLGA-po-PEG nanoparticles.

3.2. Cytotoxicity measurement

Safety and cytocompatibility are critical properties for the clinical application of a gene delivery system. Therefore, we measured the potential cytotoxicity of NP/pDNA using the CCK-8 assay. The results showed no significant cytotoxicity of the 3S-PLGA-po-PEG nanoparticles toward HAECs compared with the control group (Fig. 2a). In general, the cell viability in NP/pDNA group was relatively higher than that in Lipo group. Furthermore, due to the ability of CYP2J2-EETs to promote the proliferation of endothelial cells, the cell viability of HAECs co-cultured with the NP/pDNA complexes was over 100%, and a maximal proliferation-promoting effect was achieved at a concentration of 166.75 μg/mL. Therefore, this concentration was chosen for subsequent experiments. Our results demonstrated that nanoparticle/pDNA complexes showed no signs of cytotoxicity and could significantly stimulate the proliferation of HAECs.

3.3. Intracellular uptake and endo/lysosomal escape

For efficient gene delivery, intracellular uptake of the 3S-PLGA-po-PEG nanoparticles is necessary. Consequently, we tracked the intracellular localization of nanoparticle/coumarin-6 complexes in HAECs. According to confocal microscopy images, strong green fluorescence (coumarin-6, used for blank nanoparticles labeling) was observed in cytoplasm after 2 h of incubation (Fig. 2d), suggesting the efficient uptake of nanoparticle/coumarin-6 complexes. Successful endo/lysosomal escape is another necessary step to obtain efficient gene delivery. To assess the endo/lysosomal escape capability, the endosomes and lysosomes of HAECs were stained with LysoTracker Red. As shown in Fig. 2d, colocalizations (yellow) of endo/lysosomes and coumarin-6 were observed after 2 h of incubation, indicating the entrapment of coumarin-6 in endo/lysosomes. After 4 h of incubation, a clear green fluorescence signal was observed (Fig. 2d), suggesting the successful endo/lysosomal escape of coumarin-6 delivered by 3S-PLGA-po-PEG nanoparticles. Further plot profiles of the representative cells (Fig. 2e) confirmed the decrease in the colocalizations of the endo-/lysosomes and coumarin-6 after 4 h of incubation. All these results confirmed that coumarin-6 labeled blank nanoparticles could effectively escape from endo-/lysosomes.

3.4. In vitro transfection efficiency

Transfection efficiency exerts a crucial influence on the therapeutic effect of a gene delivery system. HAECs were incubated with nanoparticle/pDNA complexes and gene expression was analyzed via LSCM and ELISA 48 h after transfection. Using eGFP (green, used for pDNA labeling) as a reporter, LSCM observation revealed the fluorescence intensity after treatment with nanoparticle/pDNA complexes was obviously greater than that after treatment with naked pDNA and slightly weaker than that with Lipofectamine 2000 (Fig. 2b). Further quantitative ELISA analysis (Fig. 2c) showed that CYP2J2 protein expression levels after transfection with nanoparticle/pDNA complexes were significantly higher than those in the control group (41.06 ± 1.83 vs. 27.81 ± 0.56, $p < 0.001$) and naked pDNA group (41.06 ± 1.83 vs. 33.78 ± 2.15, $p < 0.001$). Moreover, there was no statistically significant difference compared with the positive control group (Lipo). Together, these results clearly showed that nanoparticle/pDNA complexes exhibited a high gene efficiency *in vitro*.

3.5. In vitro nanoparticle/pDNA complexes promoted migration and tube formation of HAECs

As endothelial cell migration is essential for angiogenesis, a scratch wound-healing assay was used to assess the effect of nanoparticle/pDNA complexes on the migration of HAECs. As shown in Fig. 3a and S2, nanoparticle/pDNA complexes significantly increased HAECs migration into the cell-free area and induced closure of scratch wounds more quickly than observed in the three other groups. An tube formation assay was also performed to evaluate the pro-angiogenic potential of the nanoparticle/pDNA complexes, and the results established that co-culture of HAECs with nanoparticle/pDNA complexes stimulated tube-like structures formation compared to the control group (Fig. 3). By virtue of higher transfection efficiency, a significant increase in tube length was seen in the presence of nanoparticle/pDNA complexes versus naked pDNA group (Fig. 3c and S3). VEGF is one of the most important angiogenic stimulators, and our results showed that naked pDNA and nanoparticle/pDNA complexes significantly promoted VEGF protein expression *in vitro*, which was consistent with previous studies [29].

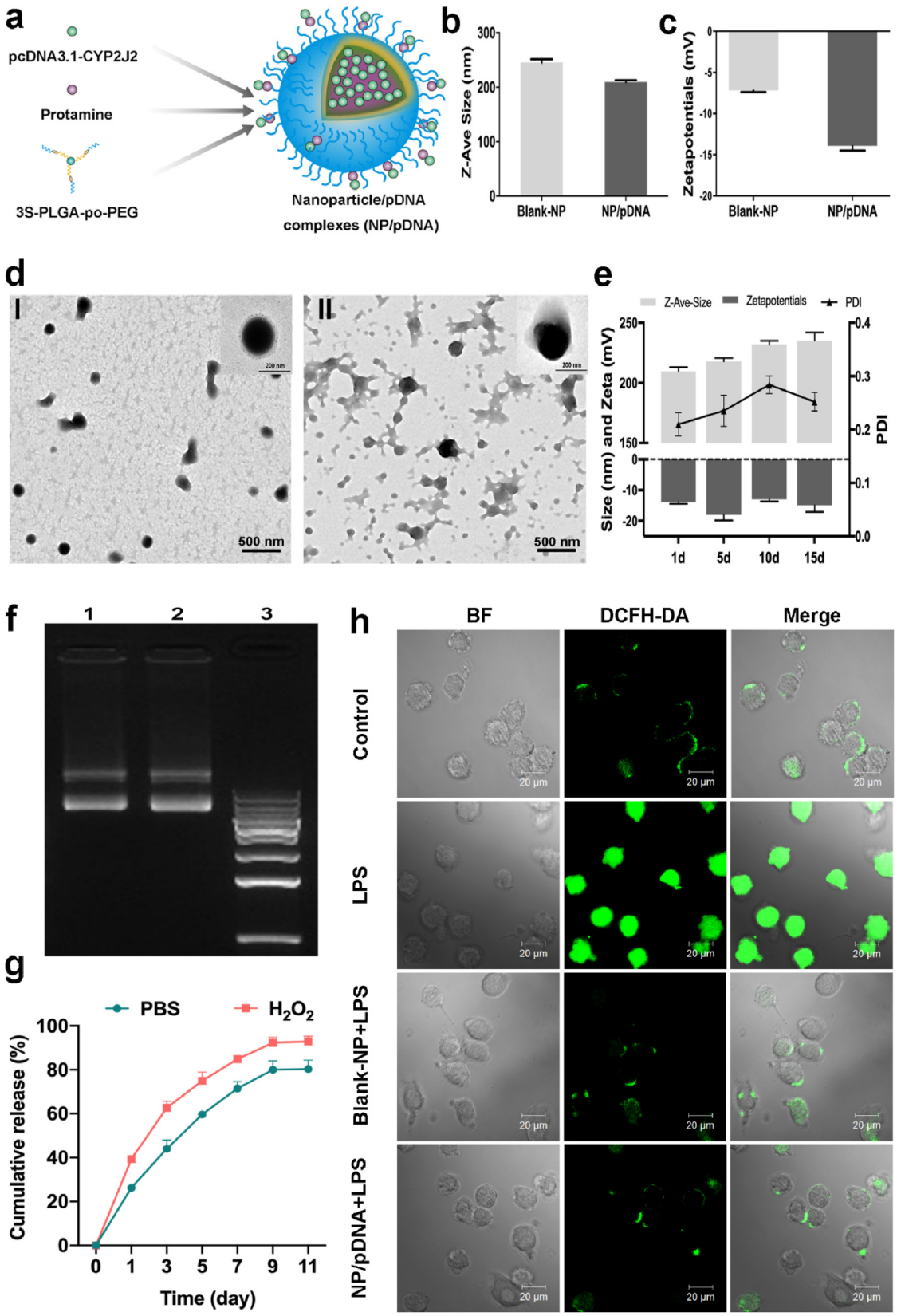

Fig. 1. Characterization of nanoparticle/pDNA complexes. (a) Schematic of nanoparticle/pDNA complex preparation. (b) Mean hydrodynamic sizes of 3S-PLGA-po-PEG and nanosphere/pDNA complexes. (c) Zeta potentials of 3S-PLGA-po-PEG and nanosphere/pDNA complexes. (d) I: TEM image of nanoparticle/plasmid complexes, II: TEM image of nanoparticle/plasmid complexes in H_2O_2 environment (Scale bars = 500 nm). (e) Zeta-potential, size and polydispersity index of nanosphere/plasmid complexes monitored by DLS. (f) Gel electrophoresis assay of pDNA extracted from nanoparticle/pDNA complexes. Lane 1: pDNA extracted from nanoparticle/pDNA complexes; Lane 2: naked pDNA; Lane 3: ladder marker. (g) *In vitro* release kinetics of pDNA from nanoparticle/pDNA complexes in PBS and H_2O_2 solution (40 μmol/L). (h) Representative LSCM images of intracellular ROS detection in HAECs (BF: bright field). Blank-NP: blank nanoparticle.

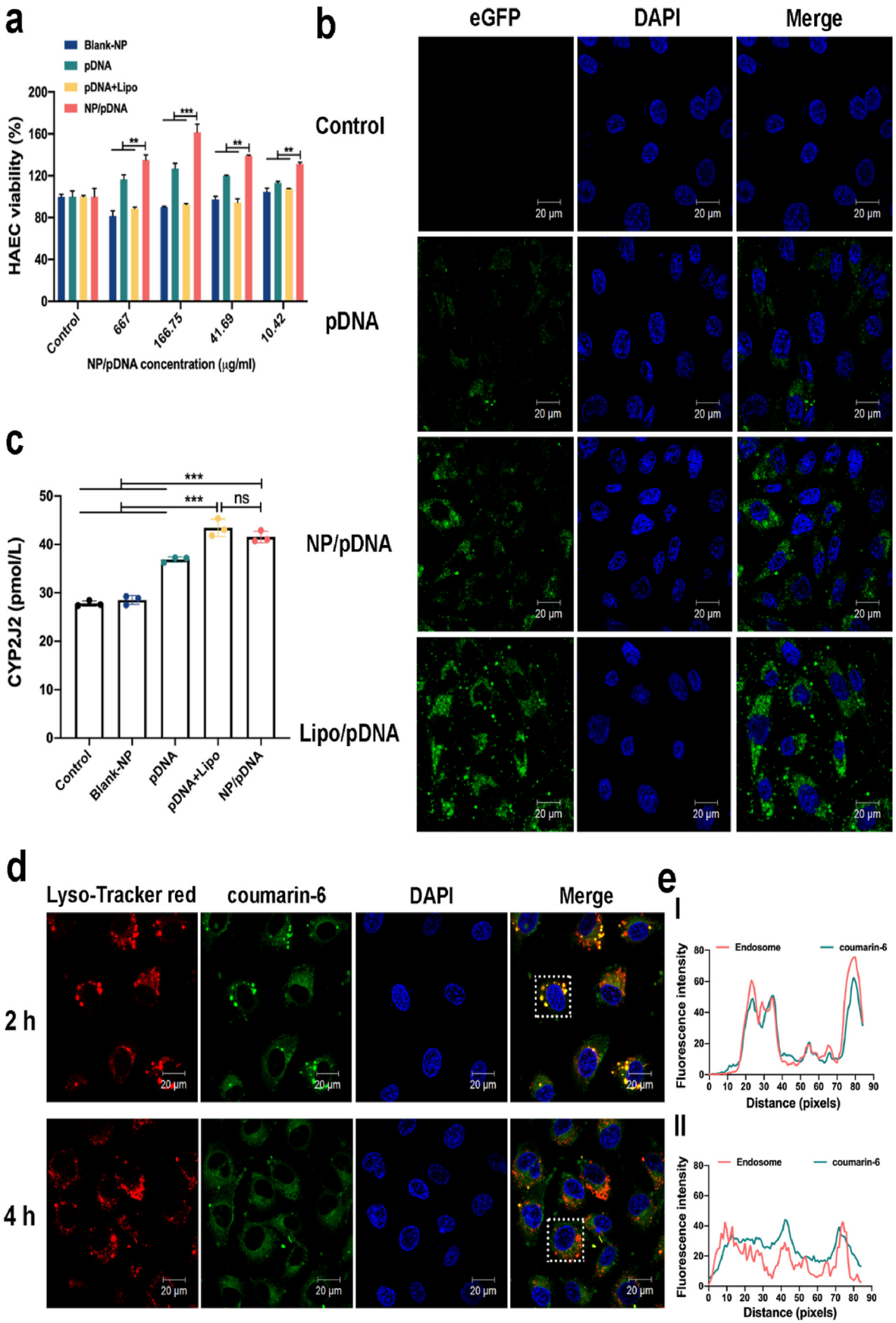

(caption on next page)

Fig. 2. *In vitro* cytotoxicity and transfection efficiency of nanoparticle/pDNA complexes in HAECs. (a) HAECs were treated with different concentrations of nanoparticle/pDNA complexes and cell viability was assessed using CCK-8 assay. The concentrations of blank-nanoparticles and naked pDNA were equal to their contents in nanoparticle/pDNA complexes. The results were expressed as the percentage of the viability of untreated control cells (100%). (b) Confocal microscopic observation of transfection efficiency. eGFP was used as a control for transfection efficiency and color intensity reflected the fluorescence intensity (Scale bars = 20 μm). (c) Quantification of CYP2J2 protein levels by ELISA. (d) Representative confocal microscopic images of intracellular uptake. HAECs were treated with coumarin-6 labeled blank-nanoparticles for 2 and 4 h (Scale bars = 20 μm; Green: coumarin-6, Blue: DAPA, Red: Lyso-Tracker Red). (e) Plot profiles of the representative cells measured using Image J (marked in rectangle; I: 2 h, II: 4 h). All results shown are representative of three independent experiments and the error bars represent standard error. Blank-NP: blank nanoparticle, pDNA: naked pDNA, NP/pDNA: nanoparticle/pDNA complex, Lipo: Lipofectamine 2000; ns: not significant, $^{*}P < 0.05$, $^{**}P < 0.01$, $^{***}P < 0.001$.

3.6. Prolonged in vivo drug retention time induced by 3s-PLGA-po-PEG nanoparticles

To assess the ability of 3S-PLGA-po-PEG nanoparticles to prolong the *in vivo* drug retention time, coumarin-6 labled 3S-PLGA-po-PEG nanoparticles were injected into ischemic gastrocnemius tissue and the fluorescence signal of coumarin-6 was monitored at different time points. As shown in Fig. 4d, coumarin-6 labled nanoparticles were distributed throughout the entire ischemic muscles 3 h after intramuscular injection, and subsequently the intensity and range of fluorescence declined from 3 to 24 h after administration. In addition, some of fluorescence signals were detected even 24 h after administration. However, in free coumarin-6 group, the fluorescence signals began to decrease after 1 h and became nearly undetectable after 24 h. Thus, 3S-PLGA-po-PEG nanoparticles prolonged the drug retention time in lower extremity muscles.

3.7. In vivo transfection efficiency

Based on the promising *in vitro* results, we explored the ability of the nanoparticle/pDNA complexes to deliver gene *in vivo*. CYP2J2 protein expression was detected via western blotting, and the results demonstrated higher CYP2J2 protein expression in the gastrocnemius muscle in NP/pDNA group (Fig. 4a and b). It is well known that 11,12-EET and 14,15-EET are the main forms of the total EET population in most cells and blood vessels [20]. Therefore, the levels of 11,12-DHET and 14,15-DHET were measured in gastrocnemius. Obviously, nanoparticle/pDNA complexes significantly increased both 11,12-DHET and 14,15-DHET levels in gastrocnemius muscle (Fig. 4c). In short, our findings confirmed the high gene delivery and expression efficiency of nanoparticle/pDNA complexes *in vivo*.

3.8. Improved blood flow and limb salvage induced by nanoparticle/pDNA complexes

Laser Doppler imaging analysis was performed to evaluate the functional blood reperfusion in the hindlimb over time. Prior to treatment, the ischemic status of hindlimb was confirmed. For non-invasive assessment of neovascularization, blood perfusion in ischemic and normal hindlimbs was tracked at days 0, 7, 14, 21 and 28 after treatment (Fig. 4e). Due to the animal inevitable individual differences, the tolerance of anesthesia varied, leading to different organ blood perfusion. The limb perfusion ratio was calculated based on the ratio of left (ischemic) to right (non-ischemic) hindlimb to ensure that the accuracy of the results was not affected by the above-mentioned limitation. As shown in Fig. 4f, nanoparticle/pDNA complex injection induced significantly enhanced blood reperfusion compared with the control and blank-nanoparticles groups at all time points post-surgery ($P < 0.05$ at day 7 and 14; $P < 0.01$ at day 21; $P < 0.001$ at day 28). Further quantitative analysis illustrated the significant recovery of blood flow in nanoparticle/pDNA group on days 7 after treatment, while further aggravated hindlimb ischemia was observed 7 days after artery excision in the control group, suggesting that early intervention is critical for the prognosis of CLI. In addition, the rate of blood perfusion in nanoparticle/pDNA complexes group was significantly higher than that in the naked-pDNA group on days 28 after intramuscular injection (0.902 ± 0.125 vs. 0.558 ± 0.06, $p < 0.05$). The physiological status of ischemic hindlimb was examined by both blood perfusion and gross appearance at the last time point (Fig. 4g and S8). Our findings revealed excellent therapeutic response and effective limb recovery in all of the mice tested ($n = 6$) in NP/pDNA group. In contrast, severe toe gangrene and muscle necrosis were clearly observed in the control group and blank nanoparticle group, and mild toe gangrene was observed in naked pDNA group. In brief, nanoparticle/pDNA complexes exhibited improved therapeutic outcomes by significantly increasing hindlimb blood reperfusion and resulted in rapid limb salvage in the mice tested.

3.9. Histological examination

The ischemic gastrocnemius muscle was harvested for histological analysis 28 days after treatment. Histological detection of H&E and Masson's trichrome-stained ischemic muscle sections demonstrated that nanoparticle/pDNA complexes obviously enhanced muscle fiber regeneration and attenuated the collagen fiber content (Fig. 5a and S5). To assess changes in vascularity, the ischemic muscle sections were immunostained for CD31, a direct marker of the levels of neo-angiogenesis. Increased CD31-positive structures were observed in both the naked pDNA and nanoparticle/pDNA groups (Fig. 5a). Moreover, quantitative analysis showed that the expression level of CD31 in the NP/pDNA group was significantly higher than that in the three other groups, indicating a superior angiogenic response induced by nanoparticle/pDNA complex treatment (Fig. 5c and S5). Since mature blood vessels consist of a single endothelial cell layer surrounded by pericytes and vascular smooth muscle cells, double immunofluorescence staining of CD31 and α-SMA (smooth muscle cell marker) was used to assess the maturity of vessels. After 28 days, only a small quantity of double-positive CD31 and α-SMA labeled vascular structures was found in the control group, blank-nanoparticles group and naked pDNA group, whereas significantly more dual-stained structures were observed in tissues treated with nanoparticles/pDNA complexes (Fig. 6a and S6). Consistent with the *in vitro* findings, VEGF protein level was significantly up-regulated in gastrocnemius muscle of tested mice treated with nanoparticle/pDNA complexes compared with mice in the three other groups (Fig. 6b and S7). Additionally, a high-level of HIF-1α (the major upstream regulator of VEGF) expression was observed in the nanoparticle/pDNA complex treated group. Moreover, the protein expression of endothelial nitric oxide synthetase (eNOS), which plays an important role in the regulation of endothelial function and vascular growth, was elevated in the NP/pDNA group. Overall, our data indicated that the nanoparticles/pDNA complex successfully induced a superior angiogenic response *in vivo*.

3.10. Potent H_2O_2-scavenging capacity and anti-inflammatory effect of nanoparticle/pDNA complexes

To investigate H_2O_2-scavenging ability of nanoparticle/pDNA complexes *in vivo*, the levels of H_2O_2 in ischemic muscle were detected by ELISA. In the control group, a high H_2O_2 level was observed, whereas in Blank-NP group and NP/pDNA group, significantly reduced H_2O_2 levels were observed (Fig. 6g). Additionally, the level of H_2O_2 in the naked pDNA group was significantly lower that of control group, but dramatically higher than that in the Blank-NP group and NP/pDNA group. To determine the role of nanoparticle/pDNA complexes in inflammation,

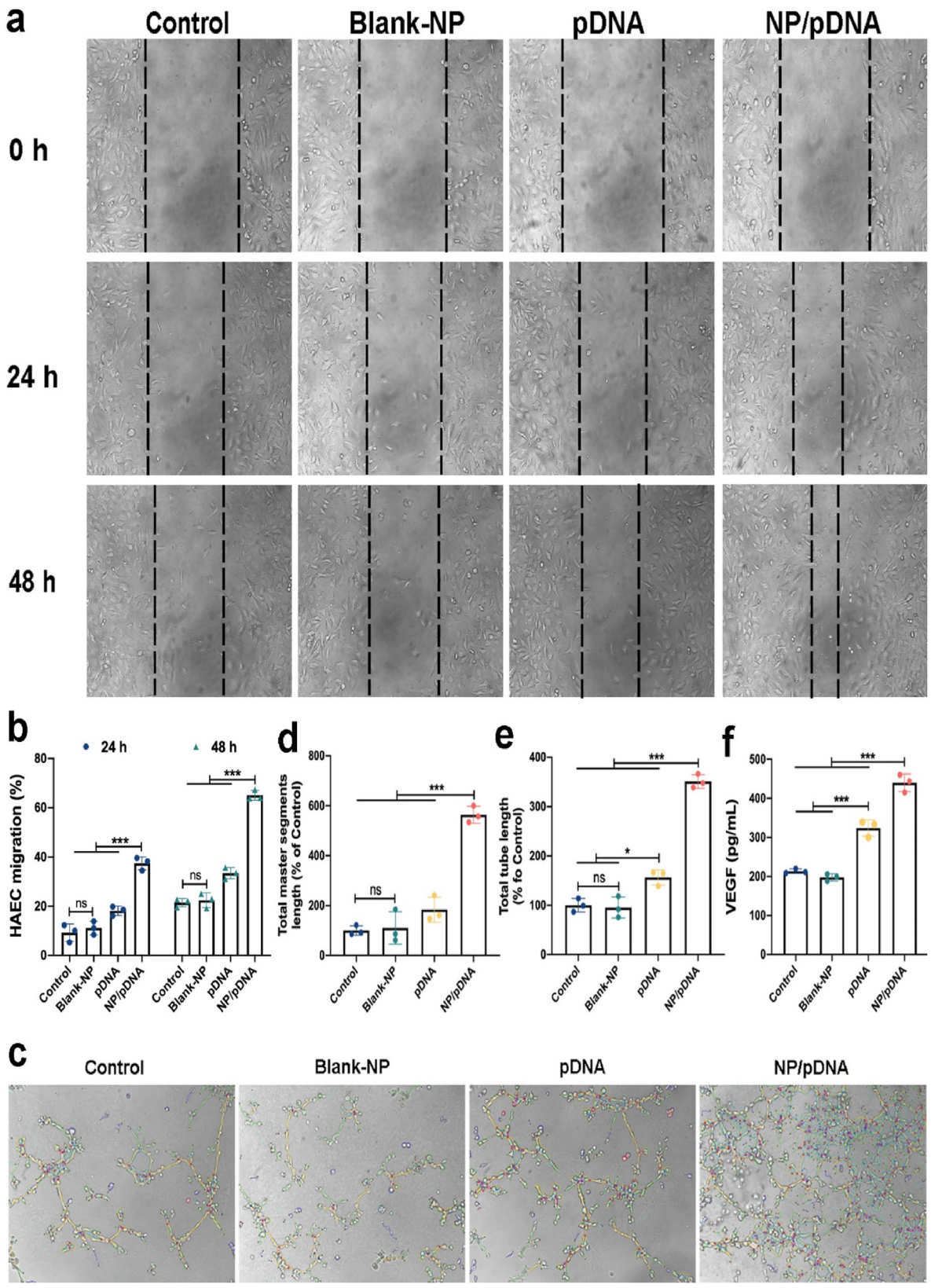

Fig. 3. Nanoparticle/pDNA complexes promoted the migration and tube formation of HAECs. (a) Representative images and (b) quantification of a scratch wound-healing assay at 0, 24 and 48 h. (c) Representative images and (d–e) quantification of Matrigel tube formation assay. (f) Cell supernatants were assayed for the protein expression of VEGF by ELISA. $n = 3$, ns: not significant, $^{*}P < 0.05$, $^{***}P < 0.001$.

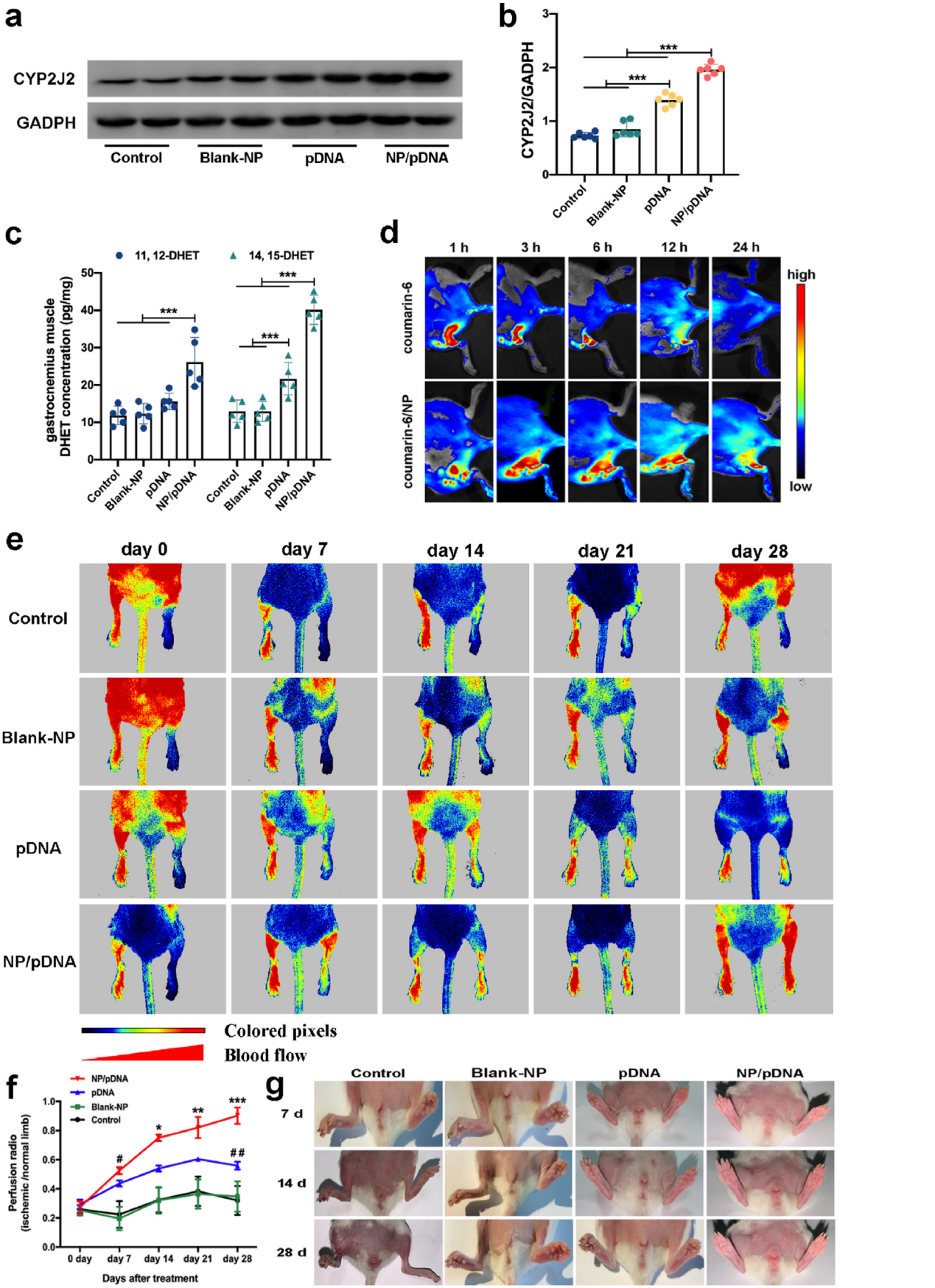

(caption on next page)

Fig. 4. *In vivo* transfection efficiency and restored ischemic limb blood flow and improved limb salvage induced by nanoparticle/pDNA complexes. (a) Western blot and (b) quantitative analysis of CYP2J2 expression in the gastrocnemius muscle of tested mice on days 7 after surgery ($n = 6$, $^{***}P < 0.001$). (c) 11, 12-DHET and 14, 15-DHET levels in mouse gastrocnemius muscle measured by ELISA ($n = 6$, $^{***}P < 0.001$). (d) Representative *in vivo* fluorescent imaging of ischemic hindlimbs treated with free coumarin-6 (green fluorescent dye) or coumarin-6/NP at the indicated time points (coumarin-6/NP: coumarin-6 labeled blank-nanoparticles). (e) Representative LDPI images of mouse hindlimbs and (f) quantitative analysis of the blood perfusion ratio (ischemic/normal) on days 0, 7, 14, 21 and 28 after treatment ($n = 6$; $^{\#}P < 0.05$ versus the Control and Blank-NP groups; $^{*}P < 0.05$ versus the Control, Blank-NP and pDNA groups; $^{**}P < 0.01$ versus the Control, Blank-NP group; $^{***}P < 0.001$ versus the Control and Blank-NP groups; $^{\#\#}P < 0.05$ versus the NP/pDNA group). (g) Physiological status of ischemic hindlimbs on days 7, 14 and 28 after treatment. Control: control group, Blank-NP: blank nanoparticle group, pDNA: naked pDNA group, NP/pDNA: nanoparticle/pDNA complex group.

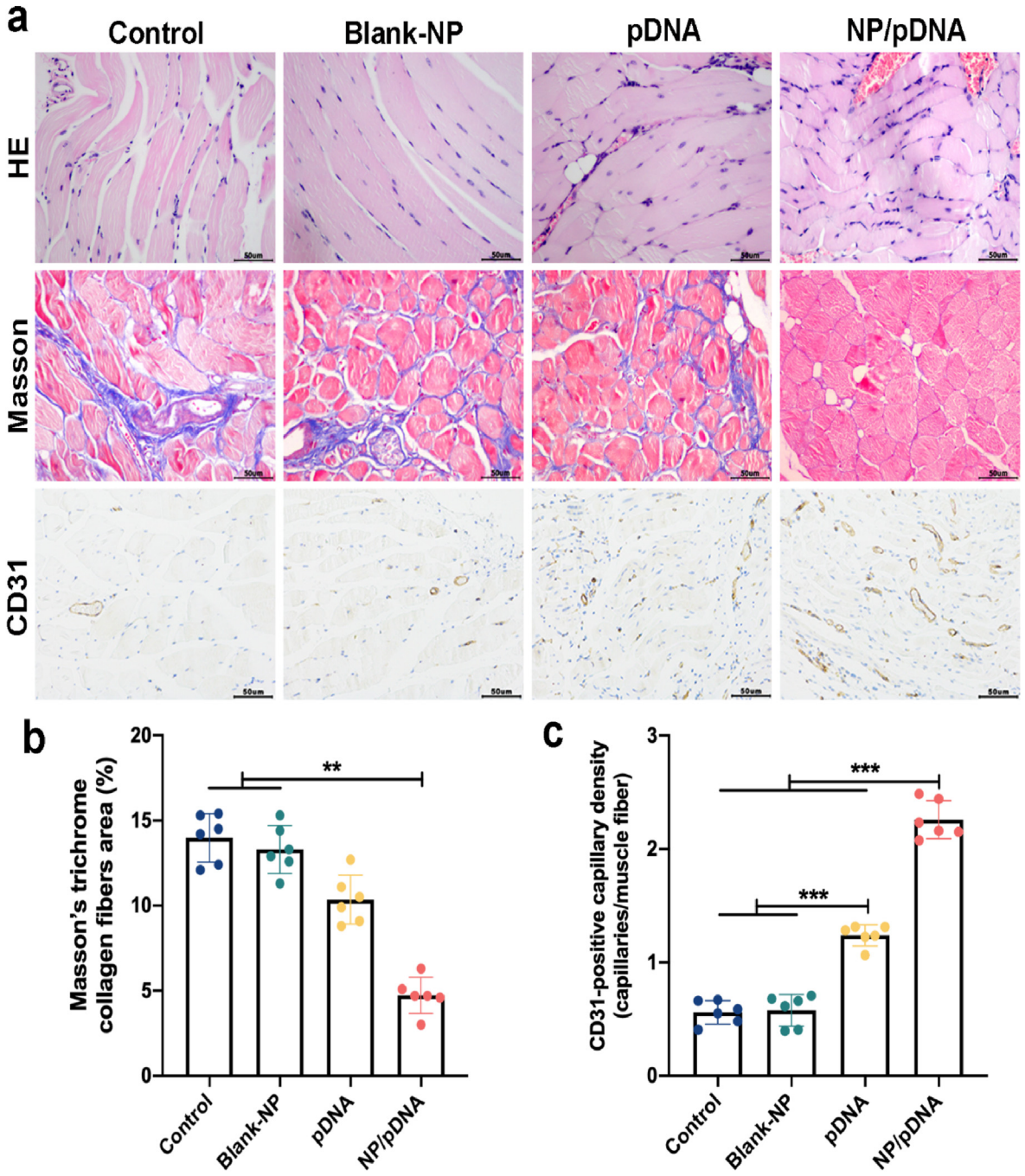

Fig. 5. *In vivo* immunohistochemical evaluation of angiogenesis. (a) Representative H&E, Masson's-trichrome and CD31 staining photomicrographs of tissue sections 28 days after treatment. (b) Quantification of Masson-trichrome analysis. (c) Quantitative analysis of CD31 stained vascular structures. $n = 6$, $^{**}P < 0.01$, $^{***}P < 0.001$.

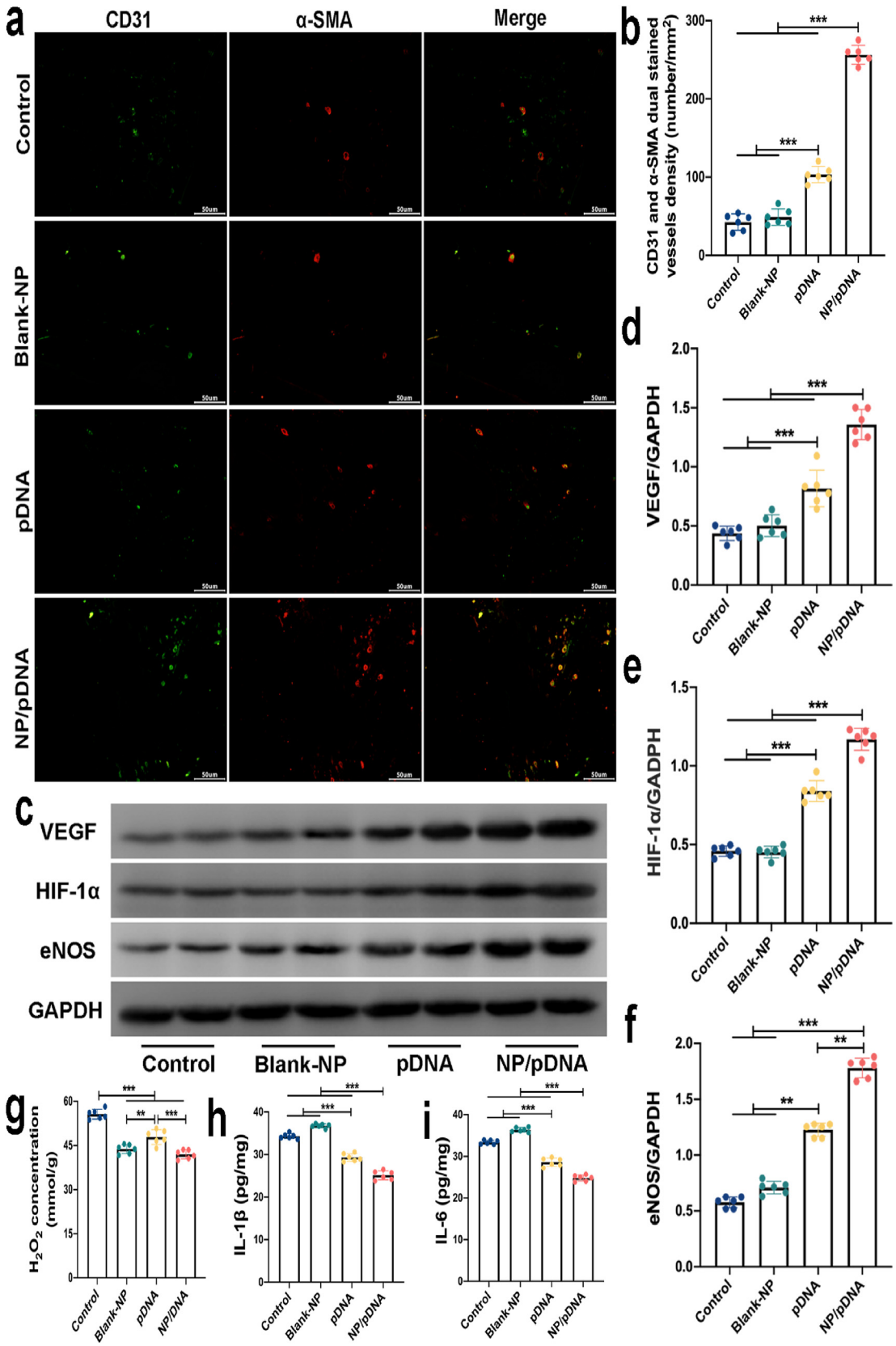

Fig. 6. *In vivo* evaluation of angiogenesis, H_2O_2-scavenging and anti-inflammatory ability of nanoparticle/pDNA complexes. (a) Representative immunofluorescence image of α-SMA (red) and CD31 (green) co-staining for evaluation of mature blood vessels 28 days after treatment. (b) Quantitative analysis of the number of CD31 and a-SMA dual stained vascular structures 28 days after treatment. (c) Representative VEGF/HIF-1α/eNOS expression in gastrocnemius tissue as assessed by western blot analyses. (d–f) Comparison of VEGF/HIF-1α/eNOS levels with GAPDH levels. (g) H_2O_2 levels in ischemic muscle measured by ELISA. (h and i) Protein levels of IL-1β and IL-6 in ischemic tissues assessed by ELISA. $n = 6$, $^{**}P < 0.01$, $^{***}P < 0.001$.

the protein levels of important pro-inflammatory factors were measured in harvested tissues using ELISA. As illustrated in Fig. 6h and i, IL-1β and IL-6 expression was remarkably inhibited after treatment with nanoparticle/pDNA complexes.

3.11. Nanoparticle/pDNA complexes efficiently improved the high oxidative stress microenvironment

HIF-1α is a pivotal stress-responsive transcription factor involved in the cellular response to hypoxia and mediates the up-regulation of hypoxia-inducible genes, such as VEGF [30,31]. In normoxia, HIF-1α is hydroxylated by prolyl hydroxylases (PHDs) with high activity and rapid degradation. Under hypoxic conditions, PHDs are inactive and HIF-1α escapes proteasomal degradation, leading to the cellular accumulation of HIF-1α. PHDs exist in three isoforms (PHD1, PHD2 and PHD3), and PHD2 plays the most important role in HIF-1α hydroxylation under normoxia [32,33]. We found that nanoparticle/pDNA complexes significantly up-regulated VEGF and HIF-1α protein expression *in vivo*. To better understand the possible mechanisms of CYP2J2/EETs-induced angiogenesis, we focused on the role of HIF-1α.

Overproduction of ROS and oxidative stress play a key role in the formation of PAD. Actually, ROS play a dual role depending on its concentration; a certain level of ROS is required, but excessive ROS production under ischemic conditions exerts inhibitory effects on neovascularization [34,35]. It has been reported that excessive ROS interferes HIF-1α accumulation by increasing PHD activity under hypoxia [36]. To investigate whether nanoparticle/pDNA complexes attenuate excess H_2O_2 to proper level, HAECs were treated with or without 20 μM H_2O_2 under hypoxic conditions (6% O_2). Similarly, hypoxia-induced accumulation of HIF-1α was reduced by an H_2O_2 mediated increase in PHD2 activity; and with strong H_2O_2 scavenging activity of 3s-PLGA-po--PEG, blank nanoparticles and nanoparticle/pDNA complexes reversed the reduction in HIF-1α accumulation by modulating PHD2 activity (Fig. 7a, d and 7e).

3.12. CYP2J2/EETs stimulated high HIF-1α expression by down-regulating PHD2 expression under hypoxia in vitro

Moreover, HIF-1α protein expression in 1the NP/pDNA group was significantly higher than that in the control and blank-NP groups while no difference in HIF-1α mRNA expression was noted among the four groups, indicating an indirect regulation of HIF-1α by CYP2J2. Given these findings, we further confirmed the expression levels of PHD2 in the presence or absence of nanoparticle/pDNA complexes. As shown in Fig. 7a and h, NP/pDNA markedly downregulated PHD2 expression. Consistent with the *in vivo* study, Western blotting analysis confirmed that nanoparticle/pDNA complexes significantly up-regulated the expression levels of HIF-1α and VEGF compared to levels in the control group; however, YC-1(a HIF-1α inhibitor) dramatically suppressed CYP2J2 induced upregulation of HIF-1α and VEGF expression (Fig. 7i). All these results revealed that reductions in the PHD2 levels allow persistence of HIF-1α, with resulting increases in HIF-1-mediated VEGF expression, which is a major mechanism of CYP2J2/EETs induced angiogenesis.

4. Discussion

With the rapidly aging population, PAD affects approximately 20% of people aged 60 and older in China, especially elderly patients with diabetes [37,38]. Moreover, the mortality rate within 5 years of CLI diagnosis is up to 50% [39]. Many advanced treatment strategies are being developed to achieve therapeutic angiogenesis for CLI patients, including pro-angiogenic factors delivery, stem cell therapy and gene therapy [40]. Among these therapeutic strategies, gene therapy has been widely studied due to its advantage of persistent growth factors expression and secretion [4,41,42]. However, existing gene therapy with pro-angiogenic factors is still not sufficient to reduce amputation and mortality rate in patients with CLI. As CLI is a multi-factorial and multi-manifested disease, there is reason to believe that gene therapy with a multiple bio-functional growth factor could achieve better therapeutic outcomes. CYP2J2 and its catalytic product EETs exhibit pleiotropic biological activities, including pro-angiogenic effect, anti-inflammation and cardiovascular protective effects [43,44], indicating that CYP2J2 could be a potential multifunctional target gene to restablish the vascular network for lower limb ischemia.

Normally, free nucleic acids are relatively quickly degraded by nucleases and the negative charge on their surface is not conducive to effectively targeting the specific cells [45]. To date, the development of low-toxic and highly efficient gene vectors has remained a huge challenge. Due to transient expression, plasmids have the disadvantage of low gene transfection efficiency [46]. Meanwhile, the potential pathogenicity of viral vectors limits their clinical application to a certain extent [9]. With the unique ability to respond intelligently to microenvironment changes, stimuli-responsive polymer gene carriers have been extensively studied in recent years [47,48]. In the present study and in our previous research, the three-arm star block copolymer-3S-PLGA-po-PEG was synthesized through ring-opening polymerization and esterification of oxalyl chloride, and the innovative method considerably shortened the reaction steps and increased the reaction efficiency [17]. As we know, the star-copolymer is composed of the tight circle and branched chains extending around the center. The highly regular structure and multiple modified sites of star-copolymer materials efficiently improve the stability of drug carriers in circulation [49,50]. It has been reported that peroxalate derivatives such as peroxalate esters (POs) can only react with hydrogen peroxide [16]. Aromatic peroxalate esters can be oxidized with hydrogen peroxide to an unstable intermediate, and the intermediate can be degraded to carbon dioxide. Due to the presence of PO, 3S-PLGA-po--PEG exhibited good anti-oxidative effect. The data in both this study and our previous research both demonstrated that 3S-PLGA-po-PEG possesses good biocompatibility, slow-release property and H_2O_2-scavenging capacity as a drug or gene carrier. Transfection efficiency is a crucial aspect of the performance of gene delivery systems [6]. In this study, both *in vitro* and *in vivo* experiments confirmed that the protein level of CYP2J2 in the nanoparticle/pDNA complex group was obviously higher compared to the other groups. Moreover, in ischemic tissues treated with nanoparticle/pDNA complexes, high CYP2J2 protein expression resulted in the significantly increased expression levels of EETs. These findings revealed the high transfection efficiency of the nanoparticle/pDNA complexes. In addition, as shown in Fig. 2, effective cellular uptake and successful endo/lysosomal escape, which exerted important roles on the therapeutic effects of nanoparticle/pDNA complexes, were observed [51,52]. To date, a wide variety of materials have been used for gene delivery, mainly including polymeric materials, polyethylenimine (PEI), inorganic materials, and numerous cationic lipid materials [40]. However, significant cytotoxic effects have been associated with PEI, cationic lipids materials and inorganic materials, making them less ideal for clinical use. Compared to previously reported non-viral gene carriers for CLI [53–56], 3S-PLGA-po-PEG not only exhibits good biocompatibility, biosafety and H_2O_2-scavenging property, but also has the ability to achieve high gene transfection efficiency. All these results strongly suggest that 3S-PLGA-po-PEG is a promising delivery vector for gene therapy for lower limb ischemia with a certain degree of novelty.

It is well known that efficient VEGF expression is essential for the application of therapeutic angiogenesis treatment in CLI [54]. VEGF is one of the target genes of HIF-1α, an inducible transcription regulator that plays an important role in intracellular oxygen homeostasis [57]. Capozzi ME et al. reported that cytochrome P450 epoxygenases (CYPs) and CYPs-derived 11, 12-EET increased VEGF production and VEGF-induced angiogenic responses following stimulation by hypoxia *in vitro* [29]. In this study, we also found that nanoparticle/pDNA complexes significantly up-regulated the VEGF protein expression *in vitro* and *in vivo*. Additionally, high expression of HIF-1α was observed in the

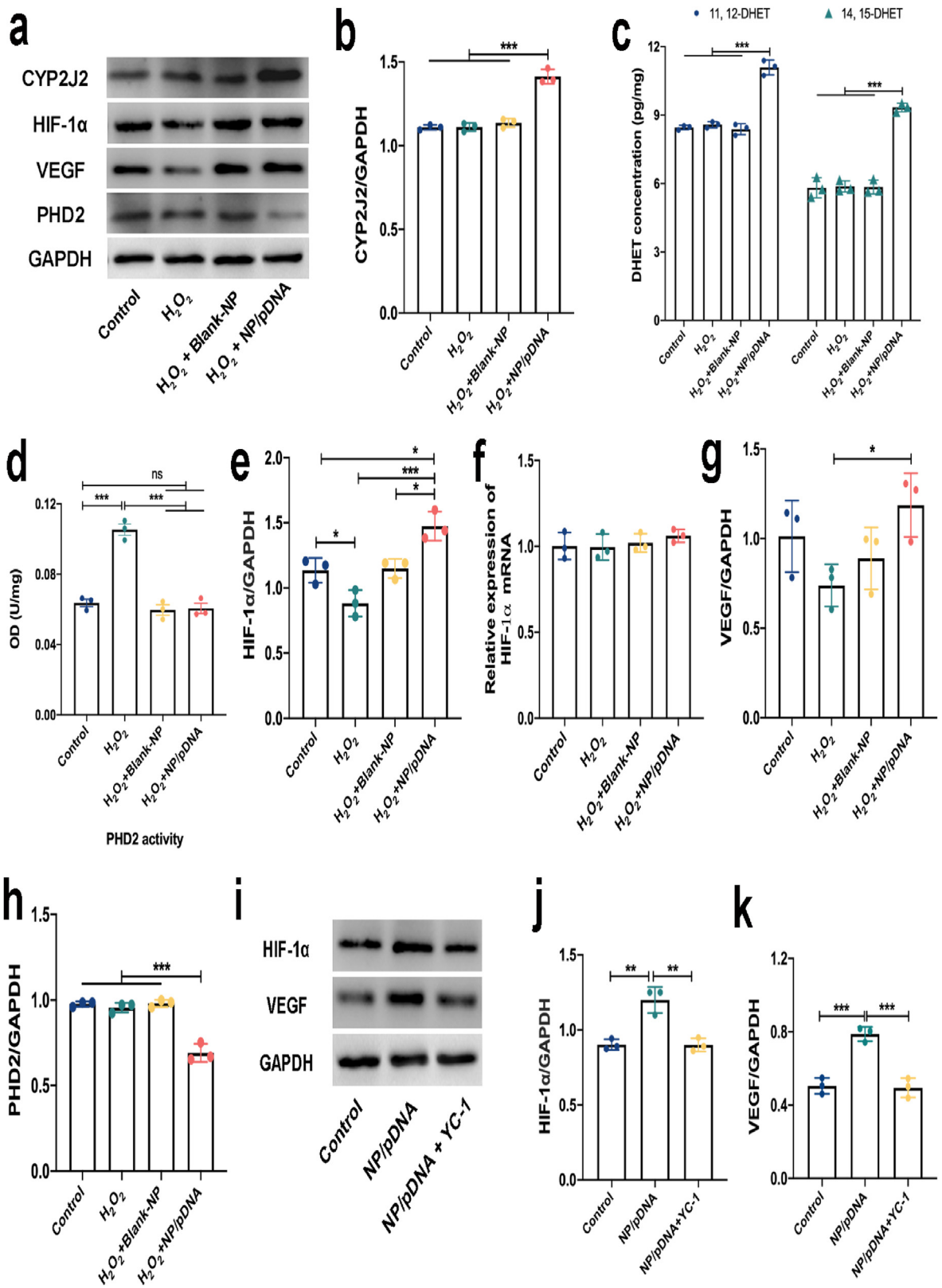

Fig. 7. HAECs were incubated with or without 20 μM H_2O_2 under hypoxic condition (6% O_2). (a) Cells were treated with 1 mL blank-nanoparticles or nanoparticle/pDNA complexes (166.75 μg/mL) for 48 h. Cell lysates were prepared and CYP2J2 (b), HIF-1α (e), VEGF (g), and PHD2 (h) protein levels were analyzed by Western blotting. (c) 11,12-DHET and 14,15-DHET were measured by ELISA. (d) PHD2 activity was determined using a spectrophotometric PHD2 Assay Kit (Genmed, Boston, MA, United States) according to the manufacturer's instructions. The readouts were measured at a wavelength of 340 nm. (f) mRNA levels of HIF-1α determined by real-time PCR analysis. (i) Cells were incubated with NP/pDNA (166.75 μg/mL) or with both NP/pDNA and YC-1 (50 μM) combined for 48 h under hypoxic. Cell lysates were subjected to Western blotting analysis for HIF-1α (j) and VEGF (k), and GAPDH for loading control. All results shown are representative of three independent experiments and the error bars represent standard error. ns: not significant, $^{*}P < 0.05$, $^{**}P < 0.01$, $^{***}P < 0.001$.

ischemic gastrocnemius of mice treated with nanoparticle/pDNA complexes. Further *in vitro* experiments showed that CYP2J2 upregulates the VEGF expression via the upstream activator HIF-1α. A decrease in PHD2 amount is important for the increased HIF-1α accumulation [58]. Surprisingly, NP/pDNA visibly decreased the PHD2 protein amount (Fig. 7). These results suggest that PHD2/HIF-1α/VEGF may be a novel signaling pathway in CYP2J2-EETs induced angiogenesis.

Histological analysis further demonstrated that nanoparticle/pDNA complexes accelerated the formation of CD31-positive neovascularization and regeneration of new muscle fibers. Moreover, a large amount of CD31 and a-SMA dual stained structures in NP/pDNA group indicated that nanoparticle/pDNA complexes could efficiently promote the maturation of vessels. Endothelial nitric oxide synthase (eNOS) functions as an important regulator of vascular tone and homeostasis through the generation of nitric oxide (NO), and the eNOS/NO pathway plays pivotal roles in the improvement of endothelial function, regulation of angiogenesis and promotion of vascular maturation [59]. Several studies have found that overexpression of CYPs (to increase the production of EETs) or treatment of cells with exogenous EETs increased the production of eNOS and NO [60,61], which is consistent with the findings of the present study. In addition, laser Doppler imaging analysis demonstrated that nanoparticle/pDNA complexes enabled rapid and strong blood reperfusion, further indicating superior pro-angiogenic effects of the nanoparticle/pDNA complexes.

Improving the ischemic micro-environment is a reasonable approach to maintain the bioactivity of target gene and enhance the therapeutic efficacy of gene delivery systems [62]. Notably, oxidative stress (OxS) and inflammation are two major pathways that contribute to the pathophysiology of PAD [63]. The high level of ROS from OxS and reduced redox capability are closely implicated in the initiation and development of PAD [64]. As reported, increased production of ROS further mediates oxidative damage to myofibers characterized by a decrease in muscle fiber cross-sectional area [64,65]. In addition, breakdown products of the ischemic tissue also trigger inflammatory response, and increased ROS levels and inflammation can mutually promote each other [66]. Consequently, treatments that target high oxidative stress and inflammatory micro-environment in ischemic tissue are very promising for improved therapeutic effects in PAD. As expected, 3S-PLGA-po-PEG has a remarkable capacity to eliminate H_2O_2 *in vitro*, resulting in reversal of the reduced HIF-1α accumulation through modulating PHD2 activity. Furthermore, with the administration of nanoparticle/pDNA complexes *in vivo*, the high level of H_2O_2 decreased to an appropriate level, which was required for angiogenesis and recovery of blood perfusion. On the other hand, several studies have shown that CYP2J2 overexpression or exogenous addition of EETs suppresses the production of TNF-α-mediated pro-inflammatory factors [67,68]. Similarly, we found that nanoparticle/pDNA complexes significantly attenuated the level production of IL-1β and IL-6 in the ischemic gastroenemius.

However, our research has a few limitations worth noting. The mouse hindlimb ischemic model is induced via acute ligation and excision of the femoral artery, which greatly contrasts with the actual clinical situation in which most cases of PAD are characterized by a chronic and progressive occlusion of the femoral-popliteal artery. In addition, further studies are needed to determine the detailed pro-angiogenic mechanism of CYP2J2 and its catalytic product EETs.

In summary, 3S-PLGA-po-PEG encapsulated plasmid pcDNA3.1-CYP2J2 exhibited excellent pro-angiogenic effects while improving high oxidative stress and inflammatory micro-environment in ischemic hindlimbs, resulting in rapid blood flow recovery and limb salvage. By virtue of multiple biological functions beneficial to post-ischemic angiogenesis, CYP2J2/EETs will likely become a new therapeutic or research target for PAD and CLI therapy. With low toxicity, high transfection efficiency and significant ROS-scavenging ability, 3S-PLGA-po-PEG nanoparticles could be a good gene delivery vector. Therefore, 3S-PLGA-po-PEG/CYP2J2-pDNA complexes have tremendous potential and provide a practical strategy for clinical PAD and CLI treatment.

Authorship contribution statement

Liang Gui: Methodology, Data curation, Visualization, Writing – original draft preparation. Youlu Chen: Conceptualization, Methodology, Data curation. Zuoguan Chen: Methodology. Jianwei Duan: Software, Visualization. Xiaoyu Liang: Software, Visualization. Huiyang Li: Methodology. Kaijing Liu: Methodology, Investigation. Yuqing Miao: Software. Qing Gao: Visualization, Investigation. Zhichao Li: Software, Validation. Yang Jing: Writing-Reviewing and Editing. Yongjun Li: Conceptualization, Supervision.

Declaration of competing interest

The authors declare that they have no known competing financial interests or personal relationships that could have appeared to influence the work reported in this paper.

Acknowledgments

This work was financially supported by the National Natural Science Foundation of China (Nos. 81870351, 82072080, 31771097); National Key Research and Development Project of China (Nos.2018YFC2000301, 2020YFC2008003); CAMS Innovation Fund for Medical Sciences (CIFMS. 2018-I2M-1–002, 2017-I2M-1–016); PUMC Discipline Construction Project (No.201920102101); Natural Science Foundation of Beijing Municipality (No.7192186); Fundamental Research Funds for the Central Universities (Nos.3332018185, 3332018174); Tianjin Research Program of Application Foundation and Advanced Technology (No.17JCZDJC37400).

Appendix A. Supplementary data

Supplementary data to this article can be found online at https://doi.org/10.1016/j.mtbio.2021.100192.

References

[1] M.H. Shishehbor, C.J. White, B.H. Gray, M.T. Menard, R. Lookstein, K. Rosenfield, M.R. Jaff, Critical limb ischemia: an expert statement, J. Am. Coll. Cardiol. 68 (18) (2016) 2002–2015.
[2] G.P. Fadini, C. Agostini, A. Avogaro, Autologous stem cell therapy for peripheral arterial disease meta-analysis and systematic review of the literature, Atherosclerosis 209 (1) (2010) 10–17.
[3] N. Idei, J. Soga, T. Hata, Y. Fujii, N. Fujimura, S. Mikami, T. Maruhashi, K. Nishioka, T. Hidaka, Y. Kihara, M. Chowdhury, K. Noma, A. Taguchi, K. Chayama, T. Sueda, Y. Higashi, Autologous bone-marrow mononuclear cell implantation reduces long-term major amputation risk in patients with critical limb ischemia: a comparison of atherosclerotic peripheral arterial disease and Buerger disease, Circ Cardiovasc Interv. 4 (1) (2011) 15–25.
[4] R.J. Powell, P. Goodney, F.O. Mendelsohn, E.K. Moen, B.H. Annex, H.G.F.T. Investigators, Safety and efficacy of patient specific intramuscular injection of HGF plasmid gene therapy on limb perfusion and wound healing in patients with ischemic lower extremity ulceration: results of the HGF-0205 trial, J. Vasc. Surg. 52 (6) (2010) 1525–1530.
[5] Y.H. Kusumanto, V. van Weel, N.H. Mulder, A.J. Smit, J.J. van den Dungen, J.M. Hooymans, W.J. Sluiter, R.A. Tio, P.H. Quax, R.O. Gans, R.P. Dullaart, G.A. Hospers, Treatment with intramuscular vascular endothelial growth factor gene compared with placebo for patients with diabetes mellitus and critical limb ischemia: a double-blind randomized trial, Hum. Gene Ther. 17 (6) (2006) 683–691.
[6] R. Shi, W. Lian, S. Han, C. Cao, Y. Jin, Y. Yuan, H. Zhao, M. Li, Nanosphere-mediated co-delivery of VEGF-A and PDGF-B genes for accelerating diabetic foot ulcers healing in rats, Gene Ther. 25 (6) (2018) 425–438.
[7] F. Sanada, Y. Taniyama, Y. Kanbara, R. Otsu, Y. Ikeda-Iwabu, M. Carracedo, H. Rakugi, R. Morishita, Gene therapy in peripheral artery disease, Expet Opin. Biol. Ther. 15 (3) (2015) 381–390.
[8] N.M. Kotchey, K. Adachi, M. Zahid, K. Inagaki, R. Charan, R.S. Parker, H. Nakai, A potential role of distinctively delayed blood clearance of recombinant adeno-associated virus serotype 9 in robust cardiac transduction, Mol. Ther. 19 (6) (2011) 1079–1089.
[9] K. Itaka, K. Kataoka, Recent development of nonviral gene delivery systems with virus-like structures and mechanisms, Eur. J. Pharm. Biopharm. 71 (3) (2009) 475–483.
[10] J. Shen, D.J. Zhao, W. Li, Q.L. Hu, Q.W. Wang, F.J. Xu, G.P. Tang, A polyethylenimine-mimetic biodegradable polycation gene vector and the effect of

amine composition in transfection efficiency, Biomaterials 34 (18) (2013) 4520–4531.
[11] W.H. De Jong, P.J. Borm, Drug delivery and nanoparticles:applications and hazards, Int. J. Nanomed. 3 (2) (2008) 133–149.
[12] M. Scalley-Kim, P. Minard, D. Baker, Low free energy cost of very long loop insertions in proteins, Protein Sci. 12 (2) (2003) 197–206.
[13] H. Shimokawa, Reactive oxygen species promote vascular smooth muscle cell proliferation, Circ. Res. 113 (2013) 104P 1042.
[14] A.L. Charles, A.S. Guilbert, M. Guillot, S. Talha, A. Lejay, A. Meyer, M. Kindo, V. Wolff, J. Bouitbir, J. Zoll, B. Geny, Muscles susceptibility to ischemia-reperfusion injuries depends on fiber type specific antioxidant level, Front. Physiol. 8 (2017) 52.
[15] M. Guillot, A.L. Charles, T.N. Chamaraux-Tran, J. Bouitbir, A. Meyer, J. Zoll, F. Schneider, B. Geny, Oxidative stress precedes skeletal muscle mitochondrial dysfunction during experimental aortic cross-clamping but is not associated with early lung, heart, brain, liver, or kidney mitochondrial impairment, J. Vasc. Surg. 60 (4) (2014) 1043–10451 e5.
[16] S.M. Silva, K. Wagner, D. Weiss, R. Beckert, C.V. Stevani, W.J. Baader, Studies on the chemiexcitation step in peroxyoxalate chemiluminescence using steroid-substituted activators, Luminescence 17 (6) (2002) 362–369.
[17] X. Zhu, C. Liu, J. Duan, X. Liang, X. Li, H. Sun, D. Kong, J. Yang, Synthesis of three-arm block copolymer poly(lactic-co-glycolic acid)-poly(ethylene glycol) with oxalyl chloride and its application in hydrophobic drug delivery, Int. J. Nanomed. 11 (2016) 6065–6077.
[18] C. Liu, X. Zhu, X. Wang, D. Miao, X. Liang, C. Wang, L. Pang, H. Sun, D. Kong, J. Yang, Hydrogen peroxide-responsive micelles self-assembled from a peroxalate ester-containing triblock copolymer, Biomater. Sci. 4 (2) (2016) 255–257.
[19] S. Wu, W. Chen, E. Murphy, S. Gabel, K.B. Tomer, J. Foley, C. Steenbergen, J.R. Falck, C.R. Moomaw, D.C. Zeldin, Molecular cloning, expression, and functional significance of a cytochrome P450 highly expressed in rat heart myocytes, J. Biol. Chem. 272 (19) (1997) 12551–12559.
[20] P.Y. Liu, Y.H. Li, T.H. Chao, H.L. Wu, L.J. Lin, L.M. Tsai, J.H. Chen, Synergistic effect of cytochrome P450 epoxygenase CYP2J2*7 polymorphism with smoking on the onset of premature myocardial infarction, Atherosclerosis 195 (1) (2007) 199–206.
[21] K. Node, Y. Huo, X. Ruan, B. Yang, M. Spiecker, K. Ley, D.C. Zeldin, J.K. Liao, Anti-inflammatory properties of cytochrome P450 epoxygenase-derived eicosanoids, Science 285 (5431) (1999) 1276–1279.
[22] W. Feng, X. Xu, G. Zhao, G. Li, T. Liu, J. Zhao, R. Dong, D.W. Wang, L. Tu, EETs and CYP2J2 inhibit TNF-alpha-induced apoptosis in pulmonary artery endothelial cells and TGF-beta1-induced migration in pulmonary artery smooth muscle cells, Int. J. Mol. Med. 32 (3) (2013) 685–693.
[23] Z. He, X. Zhang, C. Chen, Z. Wen, S.L. Hoopes, D.C. Zeldin, D.W. Wang, Cardiomyocyte-specific expression of CYP2J2 prevents development of cardiac remodelling induced by angiotensin II, Cardiovasc. Res. 105 (3) (2015) 304–317.
[24] B. Yang, L. Graham, S. Dikalov, R.P. Mason, J.R. Falck, J.K. Liao, D.C. Zeldin, Overexpression of cytochrome P450 CYP2J2 protects against hypoxia-reoxygenation injury in cultured bovine aortic endothelial cells, Mol. Pharmacol. 60 (2) (2001) 310–320.
[25] S.Y. Cheranov, M. Karpurapu, D. Wang, B. Zhang, R.C. Venema, G.N. Rao, An essential role for SRC-activated STAT-3 in 14,15-EET-induced VEGF expression and angiogenesis, Blood 111 (12) (2008) 5581–5591.
[26] W. Chen, G. Zheng, S. Yang, W. Ping, X. Fu, N. Zhang, D.W. Wang, J. Wang, CYP2J2 and EETs protect against oxidative stress and apoptosis in vivo and in vitro following lung ischemia/reperfusion, Cell. Physiol. Biochem. 33 (6) (2014) 1663–1680.
[27] X. Liang, J. Duan, X. Li, X. Zhu, Y. Chen, X. Wang, H. Sun, D. Kong, C. Li, J. Yang, Improved vaccine-induced immune responses via a ROS-triggered nanoparticle-based antigen delivery system, Nanoscale 10 (20) (2018) 9489–9503.
[28] J. Duan, Z. Chen, X. Liang, Y. Chen, H. Li, X. Tian, M. Zhang, X. Wang, H. Sun, D. Kong, Y. Li, J. Yang, Construction and application of therapeutic metal-polyphenol capsule for peripheral artery disease, Biomaterials 255 (2020) 120199.
[29] M.E. Capozzi, G.W. McCollum, J.S. Penn, The role of cytochrome P450 epoxygenases in retinal angiogenesis, Invest. Ophthalmol. Vis. Sci. 55 (7) (2014) 4253–4260.
[30] J. Gong, S. Zhou, S. Yang, Vanillic acid suppresses HIF-1α expression via inhibition of mTOR/p70S6K/4E-BP1 and raf/MEK/ERK pathways in human colon cancer HCT116 cells, Int. J. Mol. Sci. 20 (3) (2019) 465.
[31] A.E. Lin, F.C. Beasley, J. Olson, N. Keller, R.A. Shalwitz, T.J. Hannan, S.J. Hultgren, V. Nizet, Role of hypoxia inducible factor-1α (HIF-1α) in innate defense against uropathogenic Escherichia coli infection, PLoS Pathog. 11 (4) (2015), e1004818.
[32] K. Nakayama, I.J. Frew, M. Hagensen, M. Skals, H. Habelhah, A. Bhoumik, T. Kadoya, H. Erdjument-Bromage, P. Tempst, P.B. Frappell, D.D. Bowtell, Z. Ronai, Siah2 regulates stability of prolyl-hydroxylases, controls HIF1alpha abundance, and modulates physiological responses to hypoxia, Cell 117 (7) (2004) 941–952.
[33] C.A. Martinez, B. Kerr, C. Jin, P.A. Cistulli, K.M. Cook, Obstructive sleep apnea activates HIF-1 in a hypoxia dose-dependent manner in HCT116 colorectal carcinoma cells, Int. J. Mol. Sci. 20 (2) (2019) 445.
[34] J.S. Silvestre, D.M. Smadja, B.I. Lévy, Postischemic revascularization: from cellular and molecular mechanisms to clinical applications, Physiol. Rev. 93 (4) (2013) 1743–1802.
[35] M. Ushio-Fukai, Redox signaling in angiogenesis: role of NADPH oxidase, Cardiovasc. Res. 71 (2) (2006) 226–235.
[36] H. Niecknig, S. Tug, B.D. Reyes, M. Kirsch, J. Fandrey, U. Berchner-Pfannschmidt, Role of reactive oxygen species in the regulation of HIF-1 by prolyl hydroxylase 2 under mild hypoxia, Free Radic. Res. 46 (6) (2012) 705–717.
[37] Y. He, Y. Jiang, J. Wang, L. Fan, X. Li, F.B. Hu, Prevalence of peripheral arterial disease and its association with smoking in a population-based study in Beijing, China, J. Vasc. Surg. 44 (2) (2006) 333–338.
[38] L. Wang, F. Du, H. Mao, H.X. Wang, S. Zhao, Prevalence and related risk factors of peripheral arterial disease in elderly patients with type 2 diabetes in Wuhan, Central China, Chin. Med. J. (Engl) 124 (24) (2011) 4264–4268.
[39] M.G. Davies, Critical limb ischemia: introduction, Methodist. Debakey Cardiovasc. J. 8 (4) (2012) 2.
[40] C. Tu, S. Das, A.B. Baker, J. Zoldan, L.J. Suggs, Nanoscale strategies: treatment for peripheral vascular disease and critical limb ischemia, ACS Nano 9 (4) (2015) 3436–3452.
[41] F. Mac Gabhann, B.H. Annex, A.S. Popel, Gene therapy from the perspective of systems biology, Curr. Opin. Mol. Therapeut. 12 (5) (2010) 570–577.
[42] J. Belch, W.R. Hiatt, I. Baumgartner, I.V. Driver, S. Nikol, L. Norgren, E. Van Belle, T. Committees, Investigators, Effect of fibroblast growth factor NV1FGF on amputation and death: a randomised placebo-controlled trial of gene therapy in critical limb ischaemia, Lancet 377 (9781) (2011) 1929–1937.
[43] I. Fleming, R. Busse, Endothelium-derived epoxyeicosatrienoic acids and vascular function, Hypertension 47 (4) (2006) 629–633.
[44] Z. Cai, G. Zhao, J. Yan, W. Liu, W. Feng, B. Ma, L. Yang, J.A. Wang, L. Tu, D.W. Wang, CYP2J2 overexpression increases EETs and protects against angiotensin II-induced abdominal aortic aneurysm in mice, J. Lipid Res. 54 (5) (2013) 1448–1456.
[45] D. Shcharbin, V. Dzmitruk, A. Shakhbazau, N. Goncharova, I. Seviaryn, S. Kosmacheva, M. Potapnev, E. Pedziwiatr-Werbicka, M. Bryszewska, M. Talabaev, A. Chernov, V. Kulchitsky, A.M. Caminade, J.P. Majoral, Fourth generation phosphorus-containing dendrimers: prospective drug and gene delivery carrier, Pharmaceutics 3 (3) (2011) 458–473.
[46] B. Lebas, J. Galley, E. Renaud-Gabardos, F. Pujol, F. Lenfant, B. Garmy-Susini, X. Chaufour, A.C. Prats, Therapeutic benefits and adverse effects of combined proangiogenic gene therapy in mouse critical leg ischemia, Ann. Vasc. Surg. 40 (2017) 252–261.
[47] R. Mo, Z. Gu, Tumor microenvironment and intracellular signal-activated nanomaterials for anticancer drug delivery, Mater. Today 19 (5) (2016) 274–283.
[48] T. Sun, Y.S. Zhang, B. Pang, D.C. Hyun, M. Yang, Y. Xia, Engineered nanoparticles for drug delivery in cancer therapy, Angew Chem. Int. Ed. Engl. 53 (46) (2014) 12320–12364.
[49] X. Fan, Y. Zhao, W. Xu, L. Li, Linear-dendritic block copolymer for drug and gene delivery, Mater. Sci. Eng. C Mater. Biol. Appl. 62 (2016) 943–959.
[50] L. Mei, Y. Jiang, S.-S. Feng, Star-shaped block polymers as a molecular biomaterial for nanomedicine development, Nanomedicine 9 (1) (2014) 9–12.
[51] N.B.M. Ağardan, V.P. Torchilin, Chapter 1 - engineering of stimuli-sensitive nanopreparations to overcome physiological barriers and cancer multidrug resistance, in: A.M. Grumezescu (Ed.), Engineering of Nanobiomaterials, William Andrew Publishing, 2016, pp. 1–28.
[52] H. Hillaireau, P. Couvreur, Nanocarriers' entry into the cell: relevance to drug delivery, Cell. Mol. Life Sci. 66 (17) (2009) 2873–2896.
[53] H. Jiang, T. Zhang, X. Sun, Vascular endothelial growth factor gene delivery by magnetic DNA nanospheres ameliorates limb ischemia in rabbits, J. Surg. Res. 126 (1) (2005) 48–54.
[54] S.W. Kang, H.W. Lim, S.W. Seo, O. Jeon, M. Lee, B.S. Kim, Nanosphere-mediated delivery of vascular endothelial growth factor gene for therapeutic angiogenesis in mouse ischemic limbs, Biomaterials 29 (8) (2008) 1109–1117.
[55] Y. Negishi, Y. Endo-Takahashi, Y. Matsuki, Y. Kato, N. Takagi, R. Suzuki, K. Maruyama, Y. Aramaki, Systemic delivery systems of angiogenic gene by novel bubble liposomes containing cationic lipid and ultrasound exposure, Mol. Pharm. 9 (6) (2012) 1834–1840.
[56] Y. Negishi, K. Matsuo, Y. Endo-Takahashi, K. Suzuki, Y. Matsuki, N. Takagi, R. Suzuki, K. Maruyama, Y. Aramaki, Delivery of an angiogenic gene into ischemic muscle by novel bubble liposomes followed by ultrasound exposure, Pharm. Res. (N. Y.) 28 (4) (2011) 712–719.
[57] S. Gl, Life with oxygen, Science 318 (2007) 62–64.
[58] L. Zhang, Z. Sun, P. Ren, M. You, J. Zhang, L. Fang, J. Wang, Y. Chen, F. Yan, H. Zheng, M. Xie, Localized delivery of shRNA against PHD2 protects the heart from acute myocardial infarction through ultrasound-targeted cationic microbubble destruction, Theranostics 7 (1) (2017) 51–66.
[59] M. Siragusa, I. Fleming, The eNOS signalosome and its link to endothelial dysfunction, Pflügers Archiv 468 (7) (2016) 1125–1137.
[60] H. Wang, L. Lin, J. Jiang, Y. Wang, Z.Y. Lu, J.A. Bradbury, F.B. Lih, D.W. Wang, D.C. Zeldin, Up-regulation of endothelial nitric-oxide synthase by endothelium-derived hyperpolarizing factor involves mitogen-activated protein kinase and protein kinase C signaling pathways, J. Pharmacol. Exp. Therapeut. 307 (2) (2003) 753–764.
[61] R. Chen, J. Jiang, X. Xiao, D. Wang, Effects of epoxyeicosatrienoic acids on levels of eNOS phosphorylation and relevant signaling transduction pathways involved, Sci. China C Life Sci. 48 (5) (2005) 495–505.
[62] H. Bao, F. Lv, T. Liu, A pro-angiogenic degradable Mg-poly(lactic-co-glycolic acid) implant combined with rhbFGF in a rat limb ischemia model, Acta Biomater. 64 (2017) 279–289.
[63] A. Ismaeel, M.E. Franco, R. Lavado, E. Papoutsi, G.P. Casale, M. Fuglestad, C.J. Mietus, G.R. Haynatzki, R.S. Smith, W.T. Bohannon, I. Sawicki, Pipinos II, P. Koutakis, Altered metabolomic profile in patients with peripheral artery disease, J. Clin. Med. 8 (9) (2019) 1463.
[64] S.S. Signorelli, S. Scuto, E. Marino, A. Xourafa, A. Gaudio, Oxidative stress in peripheral arterial disease (PAD) mechanism and biomarkers, Antioxidants 8 (9) (2019) 367.

[65] P. Koutakis, A. Ismaeel, P. Farmer, S. Purcell, R.S. Smith, J.L. Eidson, W.T. Bohannon, Oxidative stress and antioxidant treatment in patients with peripheral artery disease, Phys. Rep. 6 (7) (2018), e13650.
[66] B.C. Dash, D. Thomas, M. Monaghan, O. Carroll, X. Chen, K. Woodhouse, T. O'Brien, A. Pandit, An injectable elastin-based gene delivery platform for dose-dependent modulation of angiogenesis and inflammation for critical limb ischemia, Biomaterials 65 (2015) 126–139.
[67] G. Zhao, J. Wang, X. Xu, Y. Jing, L. Tu, X. Li, C. Chen, K. Cianflone, P. Wang, R.T. Dackor, D.C. Zeldin, D.W. Wang, Epoxyeicosatrienoic acids protect rat hearts against tumor necrosis factor-α-induced injury, J. Lipid Res. 53 (3) (2012) 456–466.
[68] P. Shahabi, G. Siest, S. Visvikis-siest, Influence of inflammation on cardiovascular protective effects of cytochrome P450 epoxygenase-derived epoxyeicosatrienoic acids, Drug Metab. Rev. 46 (1) (2014) 33–56.